Numerical calculation of valence band structure and hole scattering rates in GaAs

Einar Halvorsen

February 11, 1991

Abstract

Software for numerical calculation of valence band structure and hole scattering rates in GaAs has been developed. The band calculation program also calculates gradients,second derivatives and eigenvectors. The rate calculations are based on a discretization of the energy band(s) using the results from the valence band structure program. The programs can easily be extended to handle strained semiconductor. Calculations of valence band structure and scattering rates in GaAs have been performed. The scattering rates have been compared to analytical parabolic results. It is found that the higher DOS in the light hole band alters the picture considerably. Considerable anisotropy have been demonstrated for ionized impurity scattering rates, due to the bandstructure effects. Similiar anisotropy effects are expected for polar optical scattering.

Contents

Chapter 1

Introduction

The Monte Carlo method has become an extensively used tool in the study of charge carrier transport in semiconductors. In a traditional Monte Carlo (MC) analysis the bandstructure of the semiconductor is described by analytical models. These models are also used to calculate transport parameters needed for a MC simulation. There are at least two cases in which these models become inadequate. When semiconductor subjected to high fields are of interest, the carriers can reach considerable energies, and the entire first Brillounzone (BZ) must be taken into account. This is not achievable with sufficient precision in the present analytical models. In order to enhance hole mobility, attention has been directed towards semiconductors subjected to strain. The valence band structure of a strained semiconductor is rather cumbersome to treat analytically except for energies very close to the band edge.

This diploma thesis is part of a larger work of which the intention is to solve these problems by treating the bandstructure numerically. To accomplish that one needs software to calculate band structure and fundamental transport parameters as scattering rates. Finally a MC program using algorithms appropriate for this representation of the physics must be developed. The main subject of this thesis will be band structure and scattering rate calculations. The latter problem is in many respects similiar to the problem of selecting a final state after scattering during simulation. A few aspects of this problem will also be mentioned.

One of the main advantages of the numerical approach is that the physical models can be altered considerably with minor programming effort. Because the bandstructure is held in look up tables, the calculation of scattering rates and the simulation of charge transport is not very dependent on the procedure used to calculate the bandstructure. Though the work presented here only includes results for unstrained GaAs the procedure for handling strained semiconductor is exactly the same from a software point of view. In fact the rate program developed is fully capable of handling strained semiconductor if the parameters are changed appropriately. Also it can easily be modified to do full zone calulations. This has not been done for two reasons. From a practical point of view it is profitable to take one step at a time. The natural starting point is then to look at carriers not far from the band edge in unstrained semiconductors. Also the theory of scattering of hot carriers is incomplete for some mechanisms, and need further development for use in high field simulations. Thus the prime task of this thesis is to shed light on the numerical algorithms and come up with scattering rates for unstrained semiconductor.

There are at least three separate works relevant to this problem. Numerical treatment of the bandstructure in MC simulations was first done by the Urbana group [1,2]. They were concerned about full zone calculations of both hole and electron transport. The primary focus was on impact ionization. Fischetti and Laux [3] went a step further by calculating scattering rates more consistent with the band model. They concentrated on high field transport of electrons in Si and GaAs. There is also a work by Hinckley and Singh [4] who have treated low field transport of holes in strained bulk GaAs. They used a 6×6 Kohn-Luttinger hamiltonian to determine the bandstructure and overlap factors. In this diploma thesis the approach of Fischetti and Laux have been combined with that of Hinckley and Singh to obtain scattering rates for GaAs more reliable than parabolic results.

In chapter 2 the fundamentals of MC simulation and the theory used for the band calculation are presented. The algorithms used are presented and discussed in chapter 3. Also a discussion of some aspects of selection of final states is given here. The results from calculations of scattering rates and band structure in GaAs are presented in chapter 4. The souce code is supplied on diskette, and user guides to the programs are given in appendix E. References are cited where appropriate.

Chapter 2

Basic theory

2.1 The Monte Carlo Method

This section describes the use of the Monte Carlo method in the study of charge carrier transport in semiconductors. It is not intended to give the full details of the method, but rather to put the work in this thesis into a context and provide explanations of important terms. In special very little is said about estimators of physical quantities. More details are available in the review articles of Price [5] and Jacoboni and Reggiani [6].

2.1.1 General

The Monte Carlo Method has become an extensively used tool in the study of charge carrier transport in semiconductors the last twenty five years. In a semi-classical description of the physics it provides a powerfull alternative to solving the Boltzmann transport equation for the system in interest. The method is based on the computer's capability to produce sequences of pseudo random numbers. It is this aspect of "gambling" that has given the method its name. The use of "random" numbers has the effect that results from Monte Carlo simulations may have a considerable variance. In this sense a simulation is more like an experiment than a straightforward numerical calculation.

The basic principles of Monte Carlo simulation of carrier transport are rather simple. A semi-classical description is used, where each carrier is assigned a Bloch state and a position at the same time. Lattice vibrations and fields from ionized impurities are treated as perturbations which may cause transitions between Bloch states, scatterings. The carriers are assumed to move according to the semi-classical equations of motion between scattering events. The carrier is assumed to be in a band, n, with dispersion relation $E_n = E_n(\vec{k})$. Letting $\vec{r}$ denote position, $\vec{k}$ wavevector, $\vec{E}$ electric field, $\vec{B}$ magnetic field and q carrier charge the equations are:

$$\vec{v} = \frac{d\vec{r}}{dt} = \frac{1}{\hbar}\nabla_{\vec{k}} E_n(\vec{k}) \tag{2.1}$$

$$\hbar\frac{d\vec{k}}{dt} = q(\vec{E} + \vec{v} \times \vec{B}) \tag{2.2}$$

The time between two subsequent scatterings of a particle is called the free flight duration. The scattering events are assumed to be instant in time. From quantum mechanics we find the scattering probability per unit time, usually called the scattering rate. This is used to generate random numbers for the duration of the free flight. Random numbers with proper distributions are also generated to select scattering mechanism and the state of the carrier after a scattering event.

There are several variants of the method. They are often divided into three cathegories:

- Single particle Monte Carlo
- Ensemble Monte Carlo
- Self consistent Monte Carlo

For space homogenous stationary problems a single particle simulation is sufficient. This is due to the ergodicity principle which states that the time average equals the ensemble average when the average is taken over an infinite time. In practice a compromise between the need for ergodicity and the cost of computer time is found. Single particle Monte Carlo is frequently used to find properties of bulk material under stationary conditions. When time dependent phenomena are of interest an ensemble Monte Carlo simulation must be performed. Then averages of physical quantities are taken over an ensemble of particles at specific instants of time. Purely space dependent problems are simulated in a similiar way, but the averages are taken over ensembles in different regions of space. The number of particles simulated is a compromize between desired variance and available computer resources. When simulating devices the electric field in the material is dependent on the distribution of the carriers, and we are usually interested in time dependent phenomena, for instance transient behaviour. Then a self consistent Monte Carlo simulation is required. This is essentially an ensemble Monte Carlo simulation where the electric field is found by solving Poisson's equation at sufficiently small time intervals.

Apart from estimating physical quantities, the tasks that are necessary to perform during a simulation falls into two cathegories: calculation of carrier trajectory and determination of scattering events. The former is found from the semi-classical equations when the electric and magnetic fields are known. The latter may be divided into three subproblems: Finding carrier free flight duration, selection of scattering mechanism and selection of final state after scattering. Determination of free flight duration is dependent on the procedure used to calculate carrier trajectory.

2.1.2 Scattering rates.

There are a number of mechanisms that may cause scattering between two Bloch states. Some mechanisms are:

- Acoustic deformation potential phonon scattering.
- Acoustic piezo-electric phonon scattering.
- Polar optical phonon scattering.
- Nonpolar optical phonon scattering.

- Ionized impurity scattering.
- Neutral impurity scatteing.
- Carrier-carrier scattering.
- Alloy scattering.

Some of these may not be present or important depending on the material. Temperature and carrier concentration also alters the relative importance of the mechanisms. The scattering process is described by first order time dependent perturbation theory. We denote the initial state of the carrier by its wavevector $\vec{k}$ and the band number n. The final state is denoted by $\vec{k}'$ and n'. We don't take spin flipping scattering into account. The probability per unit time for a transition between these two states is then given by Fermi's golden rule:

$$P^m_{nn'}(\vec{k},\vec{k}') = \frac{2\pi}{\hbar}|M^m_{nn'}(\vec{k},\vec{k}')|^2\delta(E_n(\vec{k}) + \Delta E^m - E_{n'}(\vec{k}')) \tag{2.3}$$

Here $E_n(\vec{k})$ is the dispersion relation for band nr. n. ΔE^m is the energy amount exchanged to the carrier by the interacting mechanism. This quantity might depend on the initial and final states of the carrier though it isn't shown explicitly. $M^m_{nn'}(\vec{k},\vec{k}')$ is the interaction matrix element. The scattering mechanism is denoted by m. The Fermi golden rule includes both energy and crystal momentum conservation. The energy conservation is included through the Dirac δ-distribution. The conservation of crystal momentum is is included in the squared matrix element. It has the form:

$$\vec{k} - \vec{k}' + \vec{q} = \vec{K} \tag{2.4}$$

The quantity $\vec{q}$ denotes a Fourier component of the perturbing potential. For phonon scattering it can be interpreted as $\pm$ the phonon wavevector for absorption/emission respectively. $\vec{K}$ is a reciprocal lattice vector. Scattering processes where $\vec{K} = 0$ are called normal processes. For $\vec{K} \neq 0$ we have an Umklapp process.

Very often the squared matrix element is written with a multiplicative factor called the overlap factor taken outside. If the overlap factor is denoted by $G_{nn'}(\vec{k},\vec{k}')$ we write:

$$P^m_{nn'}(\vec{k},\vec{k}') = \frac{2\pi}{\hbar}|M^m(\vec{k},\vec{k}')|^2 G_{nn'}(\vec{k},\vec{k}')\delta(E_n(\vec{k}) + \Delta E^m - E_{n'}(\vec{k}')) \tag{2.5}$$

The overlap factor is dependent on the cell periodic parts of the initial and final Bloch wavefunctions. If the Bloch wavefunction is written as $\Psi_{n,\vec{k}}(\vec{r}) = C\exp(\vec{k}\cdot\vec{r})u_{n,\vec{k}}(\vec{r})$, where C is a normalization constant and $u_{n,\vec{k}}$ is normalized to unity in the unit cell, the overlap factor is given by:

$$G_{nn'}(\vec{k},\vec{k}') = \left|\int_{cell} d^3r\, u^*_{n',\vec{k}'}(\vec{r})u_{n,\vec{k}}(\vec{r})\exp(\vec{K}\cdot\vec{r})\right|^2 \tag{2.6}$$

We usually neglect spin-flipping scattering mechanisms in simulations. When the eigenfunctions are given with spin-states, this must be accounted for. It is then appropriate to sum over final spin states and average over initial spin states . If we denote the spin states by $\mu = 1, 2$ we have:

$$G_{nn'} = \frac{1}{2}\sum_{\mu=1}^{2}\sum_{\mu'=1}^{2}\left|\int_{cell} d^3r u^*_{n'\vec{k}'\mu'}(\vec{r})u_{n\vec{k}\mu}(\vec{r})\exp(\vec{K}\cdot\vec{r})\right|^2 \tag{2.7}$$

To determine the free flight time we need the scattering rate which is the probability per unit time that a scattering event will occur. This is obtained by summing the transition probability above over all possible final states. To select scattering mechanism and final states it is convenient to treat scattering between different bands as separate mechanisms. The scattering rate of interest is then:

$$P^m_{nn'}(\vec{k}) = \sum_{\vec{k}'} P^m_{n,n'}(\vec{k},\vec{k}') \tag{2.8}$$

When calculating the scattering rate, numerically or analytically, the sum over $\vec{k}'$ is approximated by an integration. This is legitimate because the allowed k-vectors are very dense in the reciprocal space. The free flight time is found from the total scattering rate:

$$P_n(\vec{k}) = \sum_{m,n'} P^m_{nn'}(\vec{k}) \tag{2.9}$$

2.1.3 Selection of scattering mechanism.

When a simulated particle is determined to undergo a scattering at a time t, we know the wavevector $\vec{k} = \vec{k}(t)$ through equations (2.1) and (2.2) and the scattering rates for the different mechanisms for that particular value of $\vec{k}$. Of course we also know in which band n the particle is. Then we may choose among the scattering mechanisms by assigning to each a probability proportional to its scattering rate. This is rather straightforward. We generate partial sums of the form:

$$p_m = \sum_{i=1}^{m} P^i_n(\vec{k}) \tag{2.10}$$

Here i includes both different mechanisms and transitions to different bands. We define $p_0 = 0$, and for the greatest value of m we have that $p_m = P_n(\vec{k})$. Then we generate a random number, r, of uniform distribution in the interval $[0, P_n)$. The scattering mechanism selected, m, is the one satisfying :

$$p_{m-1} \leq r < p_m \tag{2.11}$$

2.1.4 Selection of final states.

When scattering mechanism is selected for a scattering event, a final state must be chosen. The possible states are those satisfying the energy conservation implied by equation (2.3). How this is accomplished is dependent on wether the bandstructure of the material is described analytically or numerically. For analytical band models it is possible to find equations for the probability distribution of the polar and azimuthal scattering angles. Then random numbers with this distribution can be generated. When scattering is isotropic, the azimuthal angle has a uniform distribution. When the bandstructure isn't described by analytical expressions, a completely different approach is needed. The algorithm for doing this is described in chapter 3.3.

2.2 Valence band calculation by the $\vec{k} \cdot \vec{p}$ method.

This section presents the fundamentals of valence band calculation by the $\vec{k} \cdot \vec{p}$ method. Everything presented here can be found in more detail in elsewhere [7,8,9]. The method is approximate, and as it is given here, it is valid in regions of $\vec{k}$-space not far from the band extremum. Spin-orbit interaction is taken into account because it has a significant impact on the valence bands. Static strain effects on the spectrum are also included. The theory is valid for semiconductors of the zincblende and diamond lattice structure provided the bandgap isn't to narrow. It should be noticed that the validity for the zincblende structure is based on the assumption that linear terms in $\vec{k}$ may be neglected in the $\vec{k} \cdot \vec{p}$ hamiltonian. This is usually considered a good approximation except for very low energies. Semiconductors of the diamond lattice structure do not contain these linear terms because of their inversion symmetry.

2.2.1 Fundamental idea

We solve a one electron problem where the state of the electron is given by :

$$H\psi = (\frac{\vec{p}^2}{2m} + V(\vec{r}))\psi = E\psi \tag{2.12}$$

Here $V(\vec{r})$ is the periodic potential of the lattice and the other electrons. Thus H is the Hartree hamiltonian. The solution of this equation is the Bloch functions:

$$\psi_{n\vec{k}}(\vec{r}) = \exp(i\vec{k} \cdot \vec{r}) u_{n\vec{k}}(\vec{r}) \tag{2.13}$$

Here n is the band index, and $\vec{k}$ is a wavevector in the first Brilloun zone (BZ). The eigenvalue for this state is denoted by $E_{n\vec{k}}$. We assume that the wavefunctions are normalized to unity in the crystal volume.

After Luttinger and Kohn we have that wavefunctions for any $\vec{k}$ may be expanded in the functions

$$\varphi_{n\vec{k}}(\vec{r}) = \exp(i(\vec{k} - \vec{k}_0) \cdot \vec{r}) \psi_{n\vec{k}_0}(\vec{r}) \tag{2.14}$$

These functions form a orthonormal basis. We let $\vec{k}_0$ be a band extremum. For the functions (2.14) we have that

$$H\varphi_{n\vec{k}}(\vec{r}) = \exp(i(\vec{k} - \vec{k}_0) H_{\vec{k}} \psi_{n\vec{k}_0}(\vec{r}) \tag{2.15}$$

where

$$H_{\vec{k}} = H + \frac{\hbar^2}{2m}(\vec{k} - \vec{k}_0)^2 + \frac{\hbar}{m}(\vec{k} - \vec{k}_0) \cdot \vec{p} \tag{2.16}$$

The hamiltonian may be written as a matrix with the functions (2.14) as a basis. The matrix elements of the hamiltonian is then given by:

$$\int_{crystal} d^3r \varphi^*_{n\vec{k}}(\vec{r}) H \varphi_{n'\vec{k}}(\vec{r}) = \left\{ E_{n\vec{k}_0} + \frac{\hbar^2}{2m}(\vec{k} - \vec{k}_0)^2 \right\} \delta_{nn'} + \frac{\hbar}{m}(\vec{k} - \vec{k}_0) \cdot \vec{p}_{nn'} \tag{2.17}$$

$$\vec{p}_{nn'} = \int_{crystal} d^3r \psi^*_{n\vec{k}_0}(\vec{r}) \vec{p} \psi_{n'\vec{k}_0}(\vec{r}) \tag{2.18}$$

The only term including interband matrix elements is the last one. For further calculations appoximations are necessary. The last term in (2.17) is treated as a perturbation. We assume that the states can be divided into two cathegories, A and B. In cathegory A we include all the bands we are interested in together with all bands interacting strongly with them. The states in cathegory B are all assumed to interact weakly with all those of cathegory A. Then we may transform the basis by a perturbative approach so that the new hamiltonian does not contain any off diagonal elements connecting states in A with states in B. The new matrix hamiltonian, $\mathcal{H}$, is referred to as the renormalized interaction matrix. To second order for degenerate bands, its elements are given by:

$$\begin{aligned} \mathcal{H}_{ij} &= \left\{ E_0 + \frac{\hbar^2}{2m}(\vec{k} - \vec{k}_0)^2 \right\} \delta_{ij} + \frac{\hbar}{m}(\vec{k} - \vec{k}_0) \cdot \vec{p}_{ij} + \\ & \frac{\hbar^2}{2m} \sum_{\alpha\beta} (\vec{k} - \vec{k}_0)_\alpha (\vec{k} - \vec{k}_0)_\beta \sum_{n' \epsilon B} \frac{p^\alpha_{in'} p^\beta_{n'j} + p^\beta_{in'} p^\alpha_{n'j}}{E_0 - E_{n'\vec{k}_0}} \end{aligned} \tag{2.19}$$

Here α and β denotes x, y or z components and E_0 is the energy of the degenerate bands at $\vec{k}_0$. The dispersion relation is then given by the matrix eigenproblem:

$$\mathcal{H}\mathcal{F} = E\mathcal{F} \tag{2.20}$$

where the eigenvector $\mathcal{F}$ is written as a column matrix. To the lowest order in $\vec{k} - \vec{k}_0$ the wavefunctions are

$$\psi_{n\vec{k}} = \exp(i(\vec{k} - \vec{k}_0) \cdot \vec{r}) \sum_j C_j \psi_{j\vec{k}_0} \tag{2.21}$$

where C_j are the components of the eigenvectors $\mathcal{F}$ obtained from (2.20).

2.2.2 Valence bands of cubic semiconductor neglecting spin.

We look at a region of $\vec{k}$-space around the Γ point $\vec{k}_0 = 0$. When spin is neglected we have a threefold degeneracy at $\vec{k} = 0$. For crystals of group T_d we neglect the linear $\vec{k}$-terms in the hamiltonian. Then we choose as a basis the Bloch functions X, Y and Z at $\vec{k}_0 = 0$ which transform under operations of the cubic group as x, y and z respectively. Group theoretic arguments are used to reduce the number of parameters necessary. Then the hamiltonian is given by

$$\begin{bmatrix} Lk_x^2 + M(k_y^2 + k_x^2) & Nk_xk_y & Nk_xk_z \\ Nk_xk_y & Lk_y^2 + M(k_x^2 + k_z^2) & Nk_yk_z \\ Nk_xk_z & Nk_yk_z & Lk_z^2 + M(k_y^2 + k_x^2) \end{bmatrix} \tag{2.22}$$

where the independent constants L, M and N are :

$$L = \frac{\hbar^2}{2m} + \frac{\hbar^2}{m^2} {\sum_n}' \frac{|< X|p_x|n >|^2}{E_0 - E_n} \tag{2.23}$$

$$M = \frac{\hbar^2}{2m} + \frac{\hbar^2}{m^2}\sum_n{}' \frac{|<X|p_y|n>|^2}{E_0 - E_n} \tag{2.24}$$

$$N = \frac{\hbar^2}{m^2}\sum_n{}' \frac{<X|p_x|n><n|p_y|Y> + <X|p_y|n><n|p_x|Y>}{E_0 - E_n} \tag{2.25}$$

2.2.3 Spin-orbit interaction.

In order to obtain results with any resemblance with reality we must include some relativistic effects in the hamiltonian. The most important is spin orbit interaction. This is done by adding a term from the Schrödinger-Pauli equation to the hamiltonian in (2.12). The hamiltonian including spin-orbit coupling is:

$$H = \frac{\vec{p}^2}{2m} + V(\vec{r}) + \frac{\hbar}{4m^2c^2}(\vec{\nabla}V \times \vec{p}) \cdot \vec{\sigma} \tag{2.26}$$

The components σ_i of $\vec{\sigma}$ are the Pauli matrices. With this new definition of H we get

$$H_{\vec{k}} = H + \frac{\hbar^2}{2m}(\vec{k} - \vec{k}_0)^2 + \frac{\hbar}{m}(\vec{k} - \vec{k}_0) \cdot \vec{\pi} \tag{2.27}$$

$$\vec{\pi} = \vec{p} + \frac{\hbar}{4mc^2}(\vec{\sigma} \times \vec{\nabla}V) \tag{2.28}$$

The basis functions must now also include spin states. We let α and β denote the spin projections $\pm\frac{1}{2}$. If we disregarded the spin orbit interaction we could have used the functions

$$X\alpha, Y\alpha, Z\alpha, X\beta, Y\beta, Z\beta \tag{2.29}$$

as a basis. Then the threefold degeneracy described in section 2.2.2 would be doubled. Instead we must use functions which diagonalize the spin-orbit term. Such functions are obtained by a unitary matrix transformation of the basis (2.29). The sixfold degeneracy is split into a fourfold and a twofold degeneracy. The appropriate functions are:

$$\psi^{3/2}_{3/2} = \frac{1}{\sqrt{2}}(X + iY)\alpha \tag{2.30}$$

$$\psi^{3/2}_{1/2} = \frac{i}{\sqrt{6}}[(X + iY)\beta - 2Z\alpha] \tag{2.31}$$

$$\psi^{3/2}_{-1/2} = \frac{1}{\sqrt{6}}[(X - iY)\alpha + 2Z\beta] \tag{2.32}$$

$$\psi^{3/2}_{-3/2} = \frac{i}{\sqrt{2}}(X - iY)\beta \tag{2.33}$$

$$\psi^{1/2}_{1/2} = \frac{1}{\sqrt{3}}[(X + iY)\beta + Z\alpha] \tag{2.34}$$

$$\psi^{1/2}_{-1/2} = \frac{i}{\sqrt{3}}[-(X - iY)\alpha + Z\beta] \tag{2.35}$$

This is called the Kohn-Luttinger representation. Equation (2.19) is still valid provided the momentum matrix elements are substituted by the matrix elements of the operator $\vec{\pi}$. In this representation the renormalized interaction matrix is :

$$\begin{bmatrix} F & H & I & 0 & \frac{i}{\sqrt{2}}H & -i\sqrt{2}I \\ H^* & G & 0 & I & \frac{i}{\sqrt{2}}(G-F) & i\sqrt{\frac{3}{2}}H \\ I^* & 0 & G & -H & -i\sqrt{\frac{3}{2}}H^* & \frac{i}{\sqrt{2}}(G-F) \\ 0 & I^* & -H^* & F & -i\sqrt{2}I^* & -\frac{i}{\sqrt{2}}H^* \\ -\frac{i}{\sqrt{2}}H^* & -\frac{i}{\sqrt{2}}(G-F) & i\sqrt{\frac{3}{2}}H & i\sqrt{2}I & \frac{1}{2}(F+G)-\Delta & 0 \\ i\sqrt{2}I^* & -i\sqrt{\frac{3}{2}}H^* & -\frac{i}{\sqrt{2}}(G-F) & \frac{i}{\sqrt{2}}H & 0 & \frac{1}{2}(F+G)-\Delta \end{bmatrix} \quad (2.36)$$

The symbol Δ denotes the spin orbit splitting at $\vec{k}=0$. The other parts are:

$$F = Ak^2 + \frac{B}{2}(k^2 - 3k_z^2) \quad (2.37)$$

$$G = Ak^2 - \frac{B}{2}(k^2 - 3k_z^2) \quad (2.38)$$

$$H = -D(k_y k_z + ik_x k_z) \quad (2.39)$$

$$I = \frac{\sqrt{3}}{2}B(k_x^2 - k_y^2) - iDk_x k_y \quad (2.40)$$

The parameters A,B and D includes the momentum matrix elements and are obtained from experimental data. For weak spin-orbit coupling they can be expressed as:

$$A = \frac{L+2M}{3} \quad (2.41)$$

$$B = \frac{L-M}{3} \quad (2.42)$$

$$D = \frac{N}{\sqrt{3}} \quad (2.43)$$

The $\vec{k}\cdot\vec{p}$ hamiltonian obtained here is not valid for narrow gap semiconductors where the spin-orbit splitting is comparable to the bandgap. For such materials the lowst conduction band must also be included in cathegory A, and a 8×8 hamiltonian is obtained.

2.2.4 Strain effects on spectrum.

The strain in a crystal is described as a tensor quantity, ε. For small and homogenous strain the tensor can be defined by

$$\varepsilon_{\alpha\beta} = \frac{1}{2}\left(\frac{\partial u_\alpha}{\partial r_\beta} + \frac{\partial u_\beta}{\partial r_\alpha}\right) \quad (2.44)$$

where $\vec{u}(\vec{r})$ is the displacement vector of a point due to strain, and α and β represent the x, y or z axes. The strain is a deformation of the crystal and might alter the type of Bravais lattice. The basis vectors of the Bravais lattice of the strained crystal, $\vec{a}_i^{\varepsilon}$, can be expressed by the strain tensor and the basis vectors for the unstrained crystal, $\vec{a}_i$:

$$\vec{a}_i^{\varepsilon} = (1+\varepsilon)\vec{a}_i \quad (2.45)$$

A small strain may be treated as a perturbation to the unstrained case. It is then necessary to perform a transformation of the coordinates of the strained crystal such that the periodicity of the crystal potential and the Bloch functions are the same as for the unstrained crystal. When spin-orbit coupling is accounted for, the result is a $\vec{k} \cdot \vec{p}$ hamiltonian of a form similiar to that given above in equation (2.36). The difference is that the terms F, G, H and I should be replaced by the following :

$$\tilde{F} = F + f \tag{2.46}$$
$$\tilde{G} = G + g \tag{2.47}$$
$$\tilde{H} = H + h \tag{2.48}$$
$$\tilde{I} = I + j \tag{2.49}$$

where the strain dependent parts are

$$f = a(\varepsilon_{xx} + \varepsilon_{yy} + \varepsilon_{zz}) + \frac{b}{2}(\varepsilon_{xx} + \varepsilon_{yy} - 2\varepsilon_{zz}) \tag{2.50}$$
$$g = a(\varepsilon_{xx} + \varepsilon_{yy} + \varepsilon_{zz}) - \frac{b}{2}(\varepsilon_{xx} + \varepsilon_{yy} - 2\varepsilon_{zz}) \tag{2.51}$$
$$h = -d(\varepsilon_{yz} + i\varepsilon_{xz}) \tag{2.52}$$
$$j = \frac{\sqrt{3}}{2} b(\varepsilon_{xx} - \varepsilon_{yy}) - id\varepsilon_{xy} \tag{2.53}$$

The deformation potentials a, b and d are obtained from experimental data.

Because of time reversal symmetry, the theory presented here will always give $E_n(\vec{k}) = E_n(-\vec{k})$, even under strain.

Chapter 3

The numerical approach.

In this chapter the algorithms used to calculate the scattering rates numerically are presented and discussed. In order to do any calculations one has to know the bandstructure of the material in interest. In addition the gradients and overlap factors are also needed. For interpolation purposes in a MC program the second derivatives of the energy must be known. Section 3.1 deals with calculation of these quantities. Section 3.2 handles the rate calculations.

3.1 Numerical calculation of valence band structure

A program KPBAND has been developed to calculate the valence band structure of GaAs by the $\vec{k} \cdot \vec{p}$ method described in chapter 2.2. This method is chosen because it makes the inclusion of strain effects simple. The eigenvectors from the $\vec{k} \cdot \vec{p}$ method are very convenient for calculation of overlap factors. For unstrained semiconductor analytical expressions exists for the overlap factors [10]. Useful expressions for strained semiconductors does not exist, however. Although the program is written to handle GaAs, it will work for any semiconductor of the diamond or zincblende structure, provided the bandgap isn't to small. Only a change of parameters is required to do this.

The program is written in Fortran 77 and should run on most computers with minor or no modifications. The subroutine which sets up the hamiltonian and solves the eigenvalue problem is based on a program written by Trond Brudevoll at the Department of Electrical Engineering and Computer Science, Norwegian Institute of Technology. This program calculated radial plots of the valence band of strained or unstrained GaAs. All other features of the program is part of the diploma work.

The output data of the program is intended for use in calculations of scattering rates and in a MC program using look-up tables for the band structure. The values computed are therefore stored in a uniform mesh of $\vec{k}$-space. Because the theory is valid only for the first tenths of an electronvolt from the band edge, only a portion of the zone is calculated. The organization of the mesh is shown in figure 3.1. For simplicity the mesh is shown only in two dimensions. The number of meshpoints along an axis (6 in the figure) together with the maximum component of a wavevector , k_{max}, along an axis can be specified to the program. The dotted lines indicates cubes in $\vec{k}$-space centered around each meshpoint. These cubes are essential for the rate calculations. The meshpoints are indicated by sollid filled circles.

In order to enhance accuracy for lower energies, the program has an option for creating an additional finer mesh around $\vec{k} = 0$.

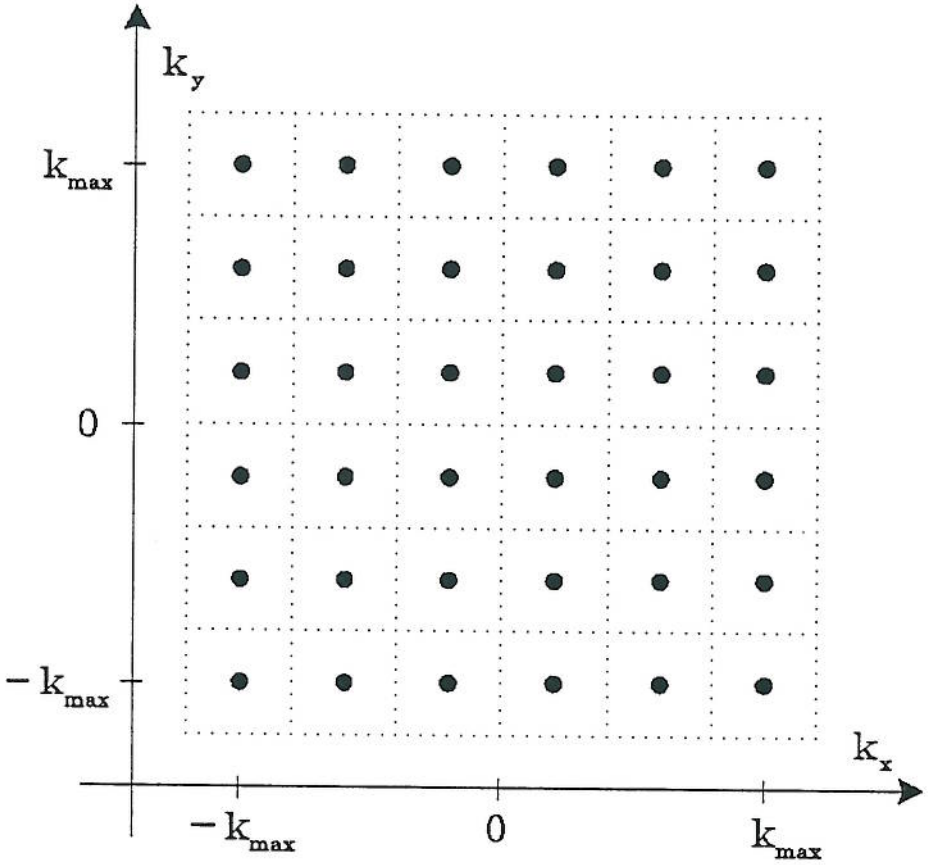

Figure 3.1: Mesh in $\vec{k}$-space.

3.1.1 Calculation of energies and eigenvectors.

The energies and eigenvectors are found by solving the eigenproblem of the 6×6 $\vec{k} \cdot \vec{p}$ hamiltonian given in chapter 2.2. Strain effects are included. This is done at each point in the mesh. The eigenproblem is solved by a routine from the NAG math library [18], which handles complex hermitian matrices. The bands are doubly degenerate due to spin, so only three different eigenvalues are obtained. For each band, both corresponding eigenvectors need to be stored, however. The energy reference is chosen such that the top of the valence band is at zero energy for unstrained semiconductor. Radial plots of the hole bands are shown in figure 3.2. The solid lines indicates unstrained semiconductor, and the dashed lines indicate strained semiconductor (strain: $\varepsilon_{xx} = \varepsilon_{yy} = 0.01, \varepsilon_{zz} = -0.009$, all other components zero). This structure with a light hole (LH) , a heavy hole (HH) and a split-off (SO) band is typical of cubic semiconductors.

The program works well for most cases, but trouble will arise when the light and heavy hole bands cross due to strain. This will only happen for special types of strain, and haven't

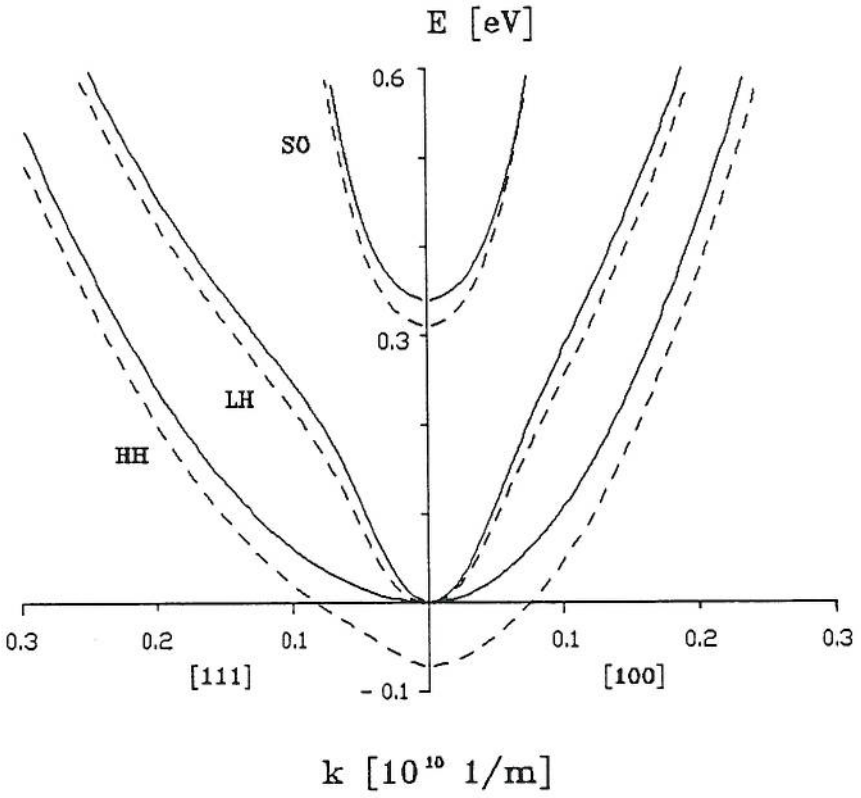

Figure 3.2: Hole dispersion relations of GaAs for two directions.

been considered relevant to this diploma thesis. Therefore no attempt has been made to overcome the problem. The trouble is caused by the fact that the NAG routine returns the eigenvectors and eigenvalues sorted in the order of increasing eigenvalues. For unstrained semiconductor the order of the bands will always be the same, but when the light and heavy hole bands cross the order in the array returned from the NAG routine will "swap". A possible way to distingush the different bands in these cases is as follows: For each set of eigenvalues and eigenvectors found, use the solution for a nearby point as a reference. Take the overlap (the sum of the squared magnitudes of the scalar products) of each of the vectors obtained with the eigenvectors of one of the bands from the reference. The two vectors giving the largest overlap must then be the two vectors belonging to this band. If the mesh isn't to coarse, values of previously calculated meshpoints can be used as references. The first meshpoint evaluated can be used as the first reference if it isn't at a point of $\vec{k}$-space where the light and heavy hole bands are degenerate with each other.

For rate calculations it is convenient to know which energies are covered by the mesh. To provide such information the program also generates the meshpoints for cubes just outside the mesh in interest. The energy spans of these cubes are then calculated by linear extrapolation. The smallest energy spanned is stored as an upper limit of energies totally enclosed by the mesh. This gives an energy limit consistent with the extrapolation method used for rate calculation. For very small meshes the time spent in this search is comparable to the time spent in generating the mesh. For a mesh of the size used in rate calculations

the overhead is small.

3.1.2 Calculation of gradients and second derivatives.

When energy is known in a uniform mesh in $\vec{k}$-space, it is possible to find the derivative with respect to any component of $\vec{k}$ by numerical methods using the values at the meshpoints around the point in interest. The disadvantage of this approach is that a significant inaccuracy may be introduced and must be checked for by some means. Calculating energies at additional points closer to the point in interest, would enhance accuracy but increase computing time considerably because it is very time consuming to solve the eigenproblem. To overcome this problem, expressions for the first and second derivatives of the energy has been found. The derivatives are expressed by the eigenvectors, eigenvalues and the derivatives of the hamiltonian matrix. Using these expressions the derivatives of the dispersion relation obtained from $\vec{k} \cdot \vec{p}$ theory can be found within machine precision. In practice the accuracy is limited by the precision of the eigenvector/eigenvalue calculation. The expressions are stated below and a deduction is given in appendix A. They have a striking similiarity with the f-sum rules [7] and could be interpreted as the $\vec{k} \cdot \vec{p}$ version of them.

$$\frac{\partial E_n}{\partial k_\alpha} = \mathcal{F}_n^* \mathcal{H}_\alpha \mathcal{F}_n \tag{3.1}$$

$$\frac{\partial^2 E_n}{\partial k_\alpha \partial k_\beta} = \mathcal{F}_n^* \mathcal{H}_{\alpha\beta} \mathcal{F}_n + 2 \sum_{\substack{i \\ E_i \neq E_n}} \frac{\Re e \left\{ (\mathcal{F}_i^* \mathcal{H}_\beta \mathcal{F}_n)(\mathcal{F}_n^* \mathcal{H}_\alpha \mathcal{F}_i) \right\}}{E_n - E_i} \tag{3.2}$$

These equations are general in the sense that they are not dependent on the kind of $\vec{k} \cdot \vec{p}$ hamiltonian used. The only assumption except for differentiability is that E_n and $\mathcal{F}_n$ constitutes an eigenpair for the hermitian matrix $\mathcal{H}$.

A similiar equation which can be used to find the derivative of the overlap factor has also been found. It has not been used in this work but may be convenient for future work. The equation is appropriate for doubly degenerate bands n and n', and arbitrary m.

$$\begin{aligned} \frac{\partial}{\partial k_\alpha} \left(|\mathcal{F}^+_{m,\vec{k}'} \mathcal{F}_{n,\vec{k}}|^2 + |\mathcal{F}^+_{m,\vec{k}'} \mathcal{F}_{n',\vec{k}}|^2 \right) = \\ 2\Re e \left\{ (\mathcal{F}^+_{m,\vec{k}'} \mathcal{F}_{n,\vec{k}})^* \sum_{\substack{i \\ E_i \neq E_n}} \frac{\mathcal{F}^+_{i,\vec{k}} \mathcal{H}_\alpha \mathcal{F}_{n,\vec{k}}}{E_n - E_i} \mathcal{F}^+_{m,\vec{k}'} \mathcal{F}_{i,\vec{k}} \right\} \\ + \quad 2\Re e \left\{ (\mathcal{F}^+_{m,\vec{k}'} \mathcal{F}_{n',\vec{k}})^* \sum_{\substack{i \\ E_i \neq E_n}} \frac{\mathcal{F}^+_{i,\vec{k}} \mathcal{H}_\alpha \mathcal{F}_{n',\vec{k}}}{E_n - E_i} \mathcal{F}^+_{m,\vec{k}'} \mathcal{F}_{i,\vec{k}} \right\} \end{aligned} \tag{3.3}$$

The derivatives of the energy could have been obtained by differentiating the secular equation. When eigenvectors are found anyway, it is very little to gain by that procedure. The approach chosen here also have the advantage of being applicable to any $\vec{k} \cdot \vec{p}$ representation of the bandstructure including full zone calculations where as much as 15 or 30 basisfunctions are used [19].

The second derivatives have not been specifically used in any calculations in this work. It has been considered most important to test the algorithm, so little effort has been made to make the calculation efficient. The second derivatives subroutine should be optimized with respect to speed before it is extensively used.

There is a problem connected with the implementation of the of the equations above that should be noticed for future work. They are relying on the eigenvectors being assigned to the correct band. If the light and heavy hole bands are degenerate with each other at a point ($\vec{k} = 0$ in unstrained GaAs), we can not distinguish the eigenvectors directly, but will have to use a procedure similiar to the one described in the previous section. This problem has no consequences for the calculations here because band extrema must be avoided in the mesh. If not, the extrapolation method described in the next section will fail.

3.2 Numerical calculation of scattering rates

A program SCRATES has been written to calculate scattering rates numerically. The program uses look-up tables for the bandstructure and related quantities. The look-up tables are organized as uniform meshes in $\vec{k}$-space as described in the previous section. The program is general in the sense that it is not dependent on the way energies and energy gradients are computed, and it will work for both holes and electrons in cubic semiconductors (except gapless semiconductors like grey tin) if parameters are changed appropriately. The most important restriction is that full zone calculations can't be done as the program is today. The reasons for this is that Umklapp processes are not taken into account and that it is difficult to calculate overlap factors properly for higher energies. Also the deformation potential theory used for acoustic and nonpolar optical phonons is valid only for lower energies and small q. Three different ways of calculating overlap factors are implemented:

- Unity overlap factor. Applicable to conduction band electrons in the lower energy regime. It can also be used where the overlap does not enter as a separate multiplicative factor.
- Analytical expressions given by Wiley [10]. These are calculated from $\vec{k} \cdot \vec{p}$ theory after Kane [11], and is applicable to holes in unstrained semiconductor.
- Overlap factors calculated from eigenvectors of the 6×6 $\vec{k} \cdot \vec{p}$ hamiltonian and applicable to holes in both strained and unstrained semiconductor.

The first breaks down at higher energies where the electron wavefunctions do not posess s-like symmetry. The others breaks down at higher energies due to the limitations of the $\vec{k} \cdot \vec{p}$ theory used.

The approach chosen is in most respects similiar to that of Fischetti and Laux [3]. The difference lies in the extents of the zone that can be calculated. Fischetti and Laux concentrated on full zone calculations of electron transport. They took Umklapp processes into account and approximated overlap factors by the rigid ion expression neglecting the band index dependence. This is not a subject for this thesis however.

3.2.1 Integrating the transition probability.

To calculate the scattering rate for a carrier scattered from a state $|\vec{k}, n>$ to a band n' by scattering mechanism m, we sum equation (2.3) over all possible $\vec{k}'$. Because of the high density of states in $\vec{k}$-space the dispersion relations may be looked upon as countinous in $\vec{k}$, and we may approximate the sum by an integral:

$$P_{nn'}(\vec{k}) = \frac{2\pi}{\hbar}\frac{V}{(2\pi)^3}\int d^3k' |M^m_{nn'}(\vec{k},\vec{k}')|^2 \delta(E_{n'}(\vec{k}') - E_n(\vec{k}) - \Delta E^m) \tag{3.4}$$

V is the crystal volume. To perform this integration numerically, we split the portion of the BZ into cubes centered around points in a uniform mesh as shown in figure 3.1. The cubes have sides of length $2b$. In each cube the energy is approximated by a linear extrapolation from the center of the cube:

$$E_{n'}(\vec{k}') = E_{n'}(\vec{k}_i) + \vec{k}'' \cdot \vec{\nabla}_{\vec{k}} E_{n'}(\vec{k}_i) \tag{3.5}$$

where

$$\vec{k}' = \vec{k}_i + \vec{k}'' \tag{3.6}$$

Here $\vec{k}_i$ denotes the centre of cube nr. i. The extrapolation is equivalent to approximate constant energy surfaces in the cube by planes normal to the gradient at the center of the cube. This is the algorithm used by Fischetti and Laux. The idea is taken from Gilat and Raubenheimer [12] who used it to calculate density of states for phonons. Now we split the final wavevector in three parts. One vector,$\vec{k}_i$, denoting the center of the cube, one vector directed along the gradient and pointing from the centre of the cube to the plane, $\vec{k}_{||}$, and one vector normal to the gradient, defining the point in the plane, $\vec{k}_\perp$.

$$\vec{k}' = \vec{k}_i + \vec{k}_{||} + \vec{k}_\perp \tag{3.7}$$

$S = S(k_{||})$ denotes the area of the constant energy plane confined by the cube. Provided the mesh is chosen fine enough we may consider ΔE^m constant within a cube. Thus we have:

$$\begin{aligned} P_{nn'}(\vec{k}) &= \frac{2\pi}{\hbar}\frac{V}{(2\pi)^3}\sum_i \int_{cube} d^3k' |M^m_{nn'}(\vec{k},\vec{k}')|^2 \, \delta(E_{n'}(\vec{k}') - E_n(\vec{k}) - \Delta E^m) \\ &\approx \frac{2\pi}{\hbar}\frac{V}{(2\pi)^3}\sum_i{}' \int dk_{||} \, \delta(E_{n'}(\vec{k}_i) + k_{||}|\vec{\nabla}_{\vec{k}} E_{n'}(\vec{k}_i)| - E_n(\vec{k}) - \Delta E^m) \\ &\quad \times \int_S d^2k_\perp |M^m_{nn'}(\vec{k},\vec{k}_i)|^2 \end{aligned} \tag{3.8}$$

The primes indicate that the sums are to be taken only over the cubes containing states of energy $E_n(\vec{k}) + \Delta E^m$ when (3.5) is used. Then energy is conserved. The integral at the right is just the integral of the squared matrix element over the cross-section area S. The average of the squared matrix element over this area is:

$$\left\langle |M^m_{nn'}(\vec{k},\vec{k}_i)|^2 \right\rangle_{S(k_{||})} = \frac{1}{S(k_{||})}\int_S d^2k_\perp |M^m_{nn'}(\vec{k},\vec{k}_i)|^2 \tag{3.9}$$

The scattering rate may now be approximated by the equation:

$$P_{nn'}(\vec{k}) = \frac{2\pi}{\hbar}\sum_i{}' D(E_n(\vec{k}) + \Delta E^m, \vec{k}_i) \left\langle |M^m_{nn'}(\vec{k}, \vec{k}_i)|^2 \right\rangle_{S(w)} \tag{3.10}$$

where

$$D(E_n(\vec{k}) + \Delta E^m, \vec{k}_i) = \frac{V}{(2\pi)^3} \frac{S(w)}{|\vec{\nabla}_{\vec{k}} E_n(\vec{k}_i)|} \tag{3.11}$$

and

$$w = \frac{E_n(\vec{k}) + \Delta E^m - E_{n'}(\vec{k}_i)}{|\vec{\nabla}_{\vec{k}} E_{n'}(\vec{k}_i)|} \tag{3.12}$$

The quantity $D(E, \vec{k}_i)$ with $w = (E - E_n(\vec{k}_i))/|\vec{\nabla}_{\vec{k}} E_n(\vec{k}_i)|$ can be interpreted as the density of states inside cube i of band n when spin is neglected. Now we see that the contribution to the scattering rate from a cube in the mesh is proportional to its DOS at the final energy and the average of the squared matrix element over the cross-section area. It is also clear that for the extrapolation method to work, there should be no zero gradients in the mesh.

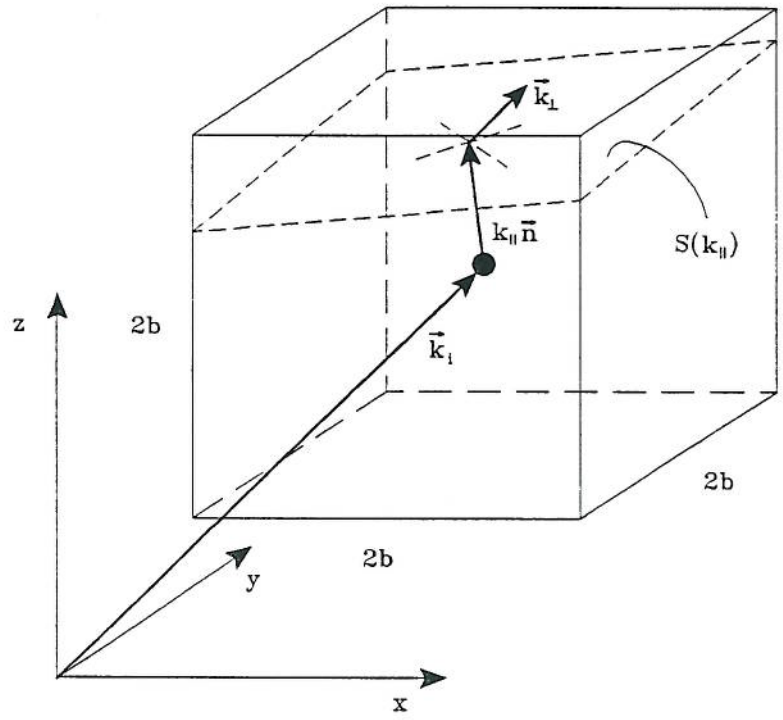

Figure 3.3: Cube centered around meshpoint.

The only quantity that remains to determine is the cross-section area. Equations for $S(w)$ have been given by Gilat and Raubenheimer [12], but contained a typographical error so they had to be recalculated. For simplicity we assume that the unit plane normal $\vec{n} = [l_1, l_2, l_3]$ has components which satisfies:

$$l_1 \geq l_2 \geq l_3 \geq 0 \tag{3.13}$$

This assumption does not impose any restrictions in practice. For a general $\vec{n}$ we just sort the magnitudes of the components to obtain a system of coordinates where (3.13) holds. For calculation of $S(w)$ no inverse transformation is required because of symmetry. We may also restrict our attention to cases for which $w > 0$ because the symmetry of the cube makes $S(w)$ an even function. Then we may list the distances of the four corners lying in this half of the cube, from the plane intersecting the center of the cube [12] :

$$\begin{aligned} w_1 &= b|l_1 - l_2 - l_3| \\ w_2 &= b(l_1 - l_2 + l_3) \\ w_3 &= b(l_1 + l_2 - l_3) \\ w_4 &= b(l_1 + l_2 + l_3) \end{aligned} \tag{3.14}$$

The equations for $S(w)$ have different form in each of the ranges $[w_{i-1}, w_i]$. There are two possibilities for $w \epsilon [0, w_1]$. The equations are:

$$S(w) = 4b^2/l_1 \ , \ \text{when } 0 < w < w_1 \text{ and } l_1 \geq l_2 + l_3 \tag{3.15}$$

$$S(w) = [l_1 l_2 l_3]^{-1}[2b^2(l_1 l_2 + l_1 l_3 + l_2 l_3) - (w^2 + b^2)] \ , \tag{3.16}$$
$$\text{when } 0 < w < w_1 \text{ and } l_1 < l_2 + l_3$$

$$S(w) = [l_1 l_2 l_3]^{-1}[b^2(3l_2 l_3 + l_1 l_2 + l_1 l_3) + wb(l_1 - l_2 - l_3) - \frac{1}{2}(w^2 + b^2)] \ , \tag{3.17}$$
$$\text{when } w_1 < w < w_2$$

$$S(w) = 2[l_1 l_2]^{-1}[b^2(l_1 + l_2) - wb] \ , \ \text{when } w_2 < w < w_3 \tag{3.18}$$

$$S(w) = [2l_1 l_2 l_3]^{-1}[b(l_1 + l_2 + l_3) - w]^2 \ , \ \text{when } w_3 < w < w_4 \tag{3.19}$$

The different shapes of the cross-section area, listed in the order above, are: parallelogram, hexagon, pentagon, quadrangle and triangle. The equation for $w \epsilon [w_1, w_2]$ is the one containing an error in reference [12]. The behaviour of $S(w)$ for two different directions of the plane normal is shown in figure 3.4. It is a continously differentiable function.

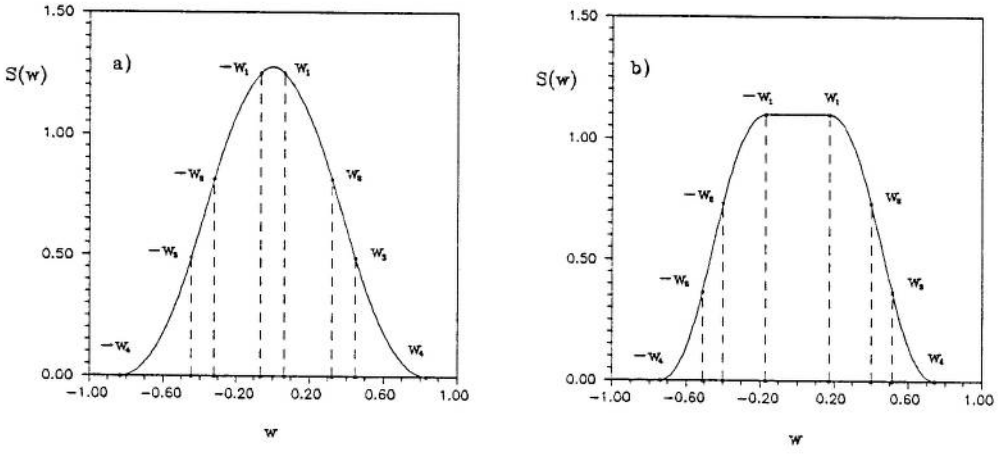

Figure 3.4: Crossection area (arbitrary units). a) $l_1 < l_2 + l_3$, b) $l_1 \geq l_2 + l_3$

Equations (3.15-3.19) have been calculated by first finding the points of the intersections between the plane and the cube edges. These points might be useful for some purposes, so they are included in appendix D.

3.2.2 Calculating squared matrix elements.

In order to determine the scattering rates, we need to know the squared matrix elements. For comparation purposes, the matrix elements used by Brudevoll et. al [13] have been implemented in the program. The scattering mechanisms are:

- Polar optical scattering, absorption and emission
- Nonpolar optical scattering, absorption and emission
- Acoustic deformation potential scattering, absorption and emission
- Ionized impurity scattering

The effect of screening is neglected for all mechanisms except ionized impurity scattering. The anisotropy of the phonon dispersion relations are ignored. An average between longitudinal and transversal modes is used for acoustic deformation potential scattering, a so called "lumped" deformation potential. For nonpolar optical scattering the three modes are assumed to have equal influence. The deformation potential mechanisms are valid in the small q approximation. For polar optical scattering only the longitudinal mode has any effect. More accurate description of the scattering processes could have been used, but then we would have to sacrifice the opportunity to compare results. The squared matrix elements excluding overlap factors are all functions of $q = |\vec{k}' - \vec{k}|$ for normal processes and are given in appendix A.

To calculate the contribution from a cube to the total rate, Fischetti and Laux have assumed that the squared matrix element varies so slowly over a cube that it to a good approximation could be regarded as constant over this variation in $\vec{k}'$. They used the centres of the initial and final cubes to determine the squared matrix element. As seen from figure 3.5, this is not necessarily a valid approximation for all scattering mechanisms. Trouble have arised when trying to calculate rates for ionized impuritiy and polar optical scattering using final states at the centers of the cubes. The trouble is caused by the nasty behaviour for small q. For polar optical phonons the great phonon energy partially solves the problem when the mesh is fine enough to ensure that there will be no transitions within a cube for intraband scattering. If the mesh is a bit to coarse, however, the initial and final states can coincide. Then we will have $q = 0$ and $|M_{nn'}|^2 = \infty$ causing trouble for the computer. For ionized impurity scattering such a transition will always be allowed because of elasticity. Fortunately the matrix element of this process does not tend to infinity as $q \to 0$. The result will be a major error in the forward scattering.

To avoid the most severe problem mentioned above, the squared matrix elements are not calculated between the initial state and the center of the cube containing the final state. instead of the cube centre, a point in the energy conserving plane (se the previous section) is chosen. For simplicity the centroid of the vertices of the cross-section area has been used. It is easily obtained from the equations in appendix D. Perhaps a more natural choice would have been the centroid of the cross-section area itself. This procedure solves the problem with polar optical phonon scattering sufficently well. For intraband ionized impurity scattering the energy conserving plane will intersect the cube centre and both the centroids will coincide with it.

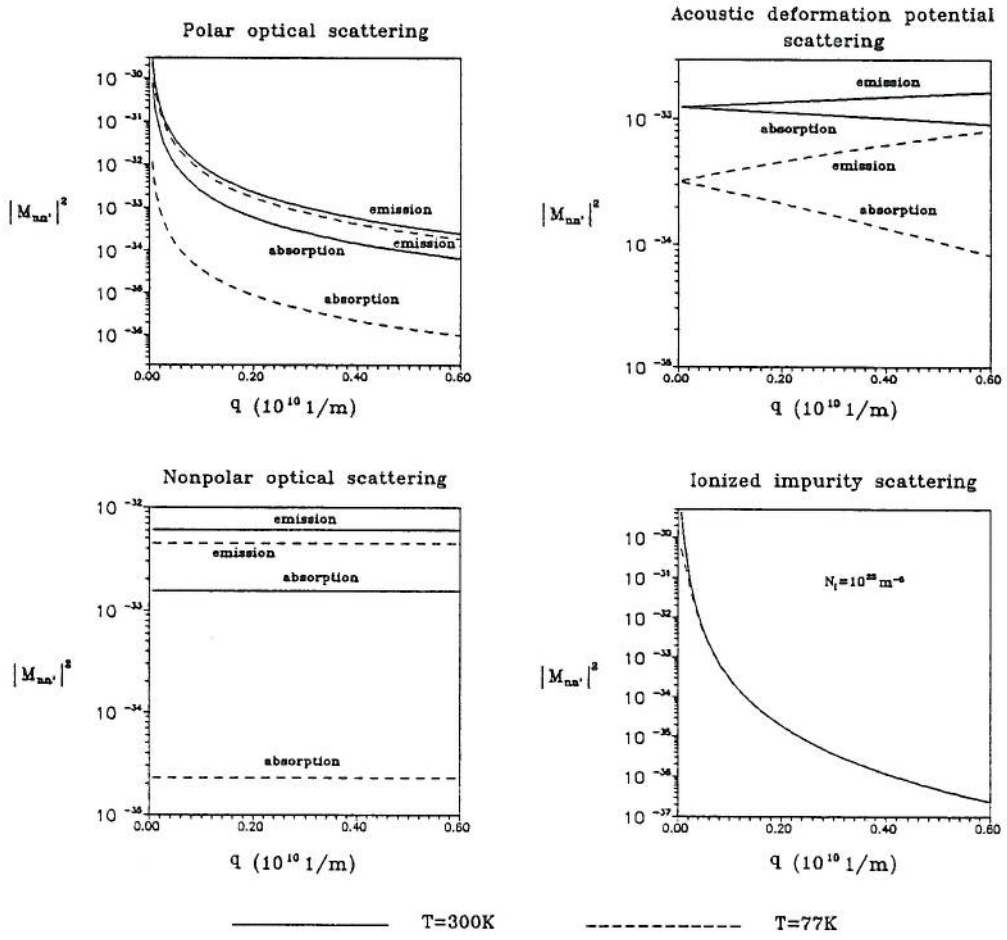

Figure 3.5: Squared matrix elements excluding overlap factors. ($|M_{nn'}|^2$ in arbitrary units.)

During an MC simulation an error in the intracube scattering for an elastic mechanism will have a very small impact on the transport properties when scattering rates and final states are computed consistently. A possible exception is for the few cubes centered around the band minimum. In this region of $\vec{k}$-space the linear extrapolation will also be rather crude. To avoid problems for lower energies there are at least two alternatives. Either one has to employ a mesh so fine that the errors are within acceptable limits, or analytical treatment near the band edge can be used. A combination is of course also possible (Fischetti and Laux [3]). A finer mesh around $\vec{k} = 0$ is implemented in SCRATES. If analytical treatment is chosen, it should be implemented in the MC-program and has no relevance to the numerical calculation of rates.

When numerically calculated rates are used together with analytically calculated angular distributions of scattering, it is not appropriate to use numerical rates which overestimate scattering within a cube or between near cubes. The reason is that it would result in an increased scattering in all possible directions, not only for the small changes in $\vec{k}'$ that have contributed to the greater numerical rate. Also we have that an overestimate of the rate will increase severly the amount of time spent to find the final state in a discrete program.

To account for this, a version of SCRATES has been written, which does a Monte Carlo averaging of the squared scattering matrix element over the energy conserving plane in a cube. This procedure works fine for rate calculations, but is totally useless for a fully discretized MC simulation because of its heavy demands on computer resources. It was meant as a temporary solution to the problem, but unfortunately this solution has been stuck at. For future work it should be replaced by analytical equations.

Both the Monte Carlo averaging and an analytical one is done by parametrizing the cross-section area. It is split into triangles wich are parametrized separately. We decompose the final k-vector into $\vec{k}_i$, a part from the cube centre to the centroid of the vertices, $\vec{v}_c$, and one from this point into any point in the triangle in interest, $\vec{v}$. Basis vectors for the parametrization are found from the vectors in appendix D. If we have two vectors, $\vec{v}_1$ and $\vec{v}_2$, defining the triangle. We may parametrize the surface by setting:

$$\vec{v} = t((1-s)\vec{v}_1 + s\vec{v}_2),\ s,t\epsilon[0,1] \tag{3.20}$$

For the MC averaging a triangle is selected with probability proportional to its area. The parameter s is found such that the angle between $\vec{v}$ and one of the basis vectors has a uniform probability distribution. Then the parameter t is found by $t = \sqrt{r}$ where r is a random number of uniform distribution. This will give a uniform probability distribution in the crossection area. A lot of such points are found, and the matrix element is averaged over all these points. This is done for scattering within a cube and to the nearest neighbours only.

For analytical determination of the average value we must integrate the squared matrix element over each triangle and divide by the total area. The integration over a trinagle is obtained by :

$$\int_{triangle} d^2k_\perp |M(q)|^2 = \frac{1}{2}|\vec{v}_1 \times \vec{v}_2| \int_0^1 ds \int_0^1 dt\, |M(q)|^2 t \tag{3.21}$$

where

$$\vec{q} = \vec{k}_i - \vec{k} + \vec{v}_c + \vec{v} \tag{3.22}$$

There is no sophistication required to perform this, but the final result will be a rather complicated expression in the basic terms. There was no time to clean up the result, implement and test it before deadline.

For most of the scattering mechanisms multiplicative overlap factors should be included. Of the three methods already mentioned, the first is trivial. The second is by equations of Wiley [10]:

$$G_{intraband}(\vec{k},\vec{k}') = \frac{1}{4}(1 + 3\cos^2\theta) \tag{3.23}$$

$$G_{interband}(\vec{k},\vec{k}') = \frac{3}{4}\sin^2\theta \tag{3.24}$$

The angle θ is between the initial and final wavevectors, and the expressions are valid for the light and heavy hole bands of an unstrained cubic semiconductor. These equations are found by simplifying more complex formulas obtained from $\vec{k}\cdot\vec{p}$ theory [11,10]. They have

the advantage of being simple, but are equivalent to results obtained from 4×4 $\vec{k} \cdot \vec{p}$ theory [20] which does not give a very realistic picture of the valence bands . The third method is just to take the squared scalar product of the eigenvectors obtained from more precise $\vec{k} \cdot \vec{p}$ calculations (6×6 in this work). This has been done by Hinckley and Singh [4]. The approach is correct to lowest order in $\vec{k}$ when Umklapp processes are not taken into account. For these processes one has to include the matrix elements of $\exp(i\vec{K} \cdot \vec{r})$ between the basis functions of the hamiltonian matrix. Umklapp processes don't have any significance when only a rather small portion of the BZ is of interest.

In the representation used here, spin is accounted for in the band calculations, but spin-flipping is neglected in the models of the scattering processes. It should be noticed that the eigenvectors obtained for a band from the program KPBAND do not represent clean spin up and spin down states, but different mixtures of these. If we let n mean the band number and $\mathcal{F}_{n\mu\vec{k}}$ an eigenvector for this band, where $\mu = 1, 2$ denotes the different mixtures of spin states, equation (2.7) gives the overlap factor:

$$G_{nn'}(\vec{k}, \vec{k}') = \frac{1}{2} \sum_{\mu=1}^{2} \sum_{\mu'=1}^{2} |\mathcal{F}^{+}_{n'\mu'\vec{k}'} \mathcal{F}_{n\mu\vec{k}}|^2 \tag{3.25}$$

Polar plots of overlap factors for GaAs are given in figures 3.6 and 3.7. Only heavy to heavy and heavy to light hole transitions are shown. Light to light and light to heavy hole transitions have qualitatively the same behaviour. The solid curves are overlap factors calculated by equation (3.25). The dashed curves indicate overlap factors calculated by equations (3.23) and (3.24). It should be noticed that for unstrained semiconductor the numerical results will coincide with the analytical when the wavevectors are very close to $\vec{k} = 0$. For strained semiconductor (figure 3.7) the behaviour of $G_{nn'}$ is qualitatively

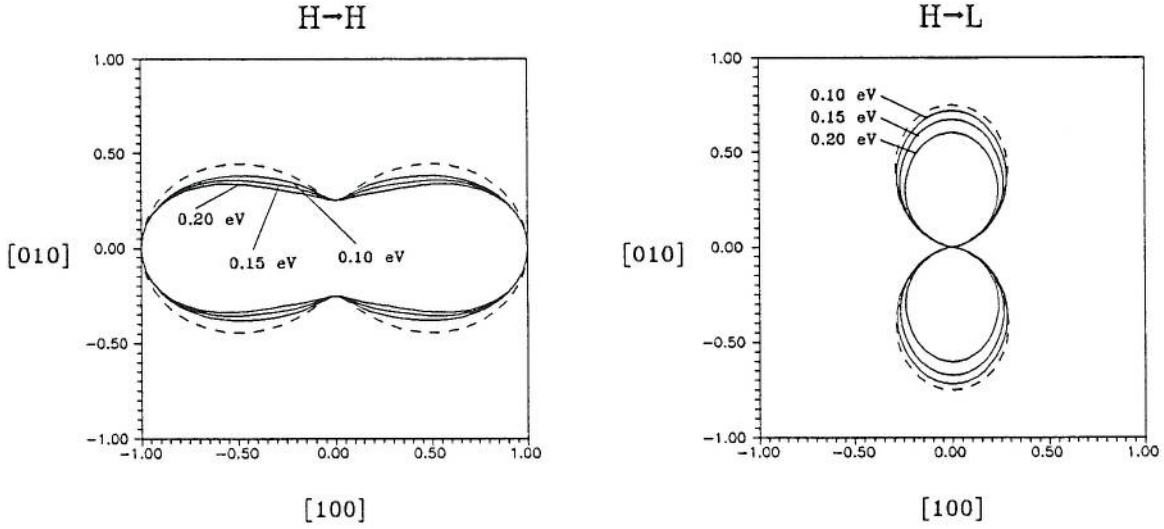

Figure 3.6: Polar plot of overlap factors for unstrained GaAs. (Inital state at 0.15 eV and wavevector along [100]. Final energies given in figure.)

different. There is a loss of symmetry, and the overlap factors can not be approximated by the analytical expressions (3.23,3.24).

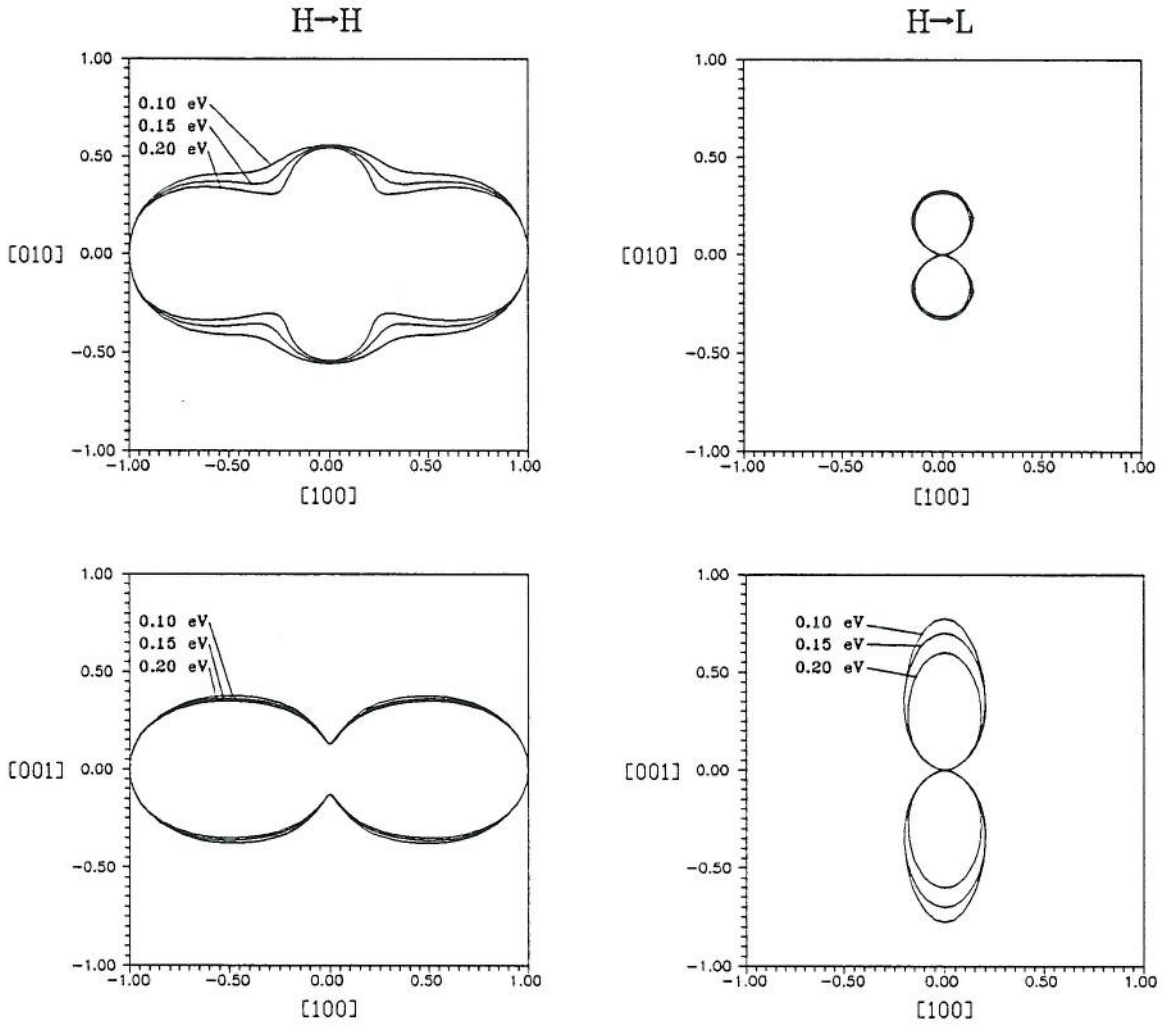

Figure 3.7: Polar plot of overlap factors for strained GaAs. (Inital state at 0.15 eV and wavevector along [100]. Final energies given in figure.)

The program flow is rather simple. For each initial state the mesh of final states is searched to find the cubes containing the desired final energy. If a finer mesh around $\vec{k} = 0$ is present, the energy limit of the fine mesh is used to decide wether the search should be done in the fine or the coarse mesh. The energy span of each cube have been stored in look up tables at the start of the program. The span is calculated by linear extrapolation. Then the contributions from all cubes are added as in equation 3.10. The average squared matrix element for each cube is estimated by taking the centroid of the cross-section vertices as final state. The overlap factor is calculated separately. When eigenvectors are used the overlap factors are calculated between initial state and the centre of the final cube. When analytical equations are used the same final state as used for the rest of the matrix element is used. For the mesh sizes of interest the overlap factors are rather slowly varying from meshpoint to meshpoint and need not be part of the averaging used for the illbehaved mechanisms.

For rate calculations during this work several versions of SCRATES have been made to test algorithms and to fit special needs. The supplied version is the "mother" program. The MC averaging subroutines are supplied separately. The searching algorithm used has been a "brute force" search. This has been done because it was the only way found suitable to handle inelastic acoustic deformation potential scattering. A faster searching algorithm should be used for the other mechanisms in the future when calculations of rates are to be done for a vast number of points.

3.3 Selection of final states

Though no software work has been done on the problem of selection of final states, a few thoughts on how this is done are appropriate to include. In the discrete MC simulation the determination of final states is done in two parts. This is described by Fischetti and Laux. First a cube containing the final state is chosen. This is done by the rejection method [6], where each cube is assigned a statistical weight according to its DOS and the average of the squared matrix element over this cube (the value at the cube centre in their work). Then one must find a k-vector preferably in this cube wich represent the desired energy with a sufficient precision. Just selecting the cube centre would be profitable for effeciency, but can cause unacceptable errrors in the final energy giving an artificial heating or cooling of the carriers. Fischetti and Laux have used a second order interpolation between the eight nearest meshpoints to avoid the problem. This interpolation is then inverted to third order along predetermined directions.

The task of finding the final cube is very critical during simulation. In principle we could do this the same way we choose scattering mechanism. Then we would have to calculate the weights for all the possible final cubes. There can be several thousands of final cubes for a given initial state. The time consumed calculating weights for all these cubes could be devastating to the efficiency of the MC program. Fischetti and Laux therefore use a rejection method to determine the final cube. Then there is no need to compute all the weights.

The problem is not entirely solved by this procedure, however. Some of the scattering mechanisms (especially ionized impurity scattering) are strongly dependent on the magnitude of q. For this mechanisms there will be a very strong variation of the weights from cube to cube. Figure 3.8 illustrates the problem. This figure shows the weights of each final cube as a function of the cube number. It is for intraband heavy hole scattering with initial energy 0.10 eV and k-vector on the [100] axis. The mesh contains 24^3 points.

The order in which the cubes appear is dependent on the algorithm used to search the mesh. The high degree of symmetry in the figure is caused by the position of the initial state with respect to the mesh. Figure 3.8 shows the weights of the final cubes for the same scattering process and initial energy, and with $\vec{k}$ along the [111] axis. The rejection method will have a tremendous high rate of rejections if it is applied directly. The problem is caused by the strong variation in the matrix element for small q. This problem will also occur for intraband polar optical scattering. Interband scattering by these mechanism will not cause trouble to the same extent because the forward scattering is suppressed by the form of the overlap integral. Thus a much smaller deviation in the weights are obtained. The other scattering mechanisms will aslo be rather well behaved compared to intraband

ionized impurity and polar optical scattering.

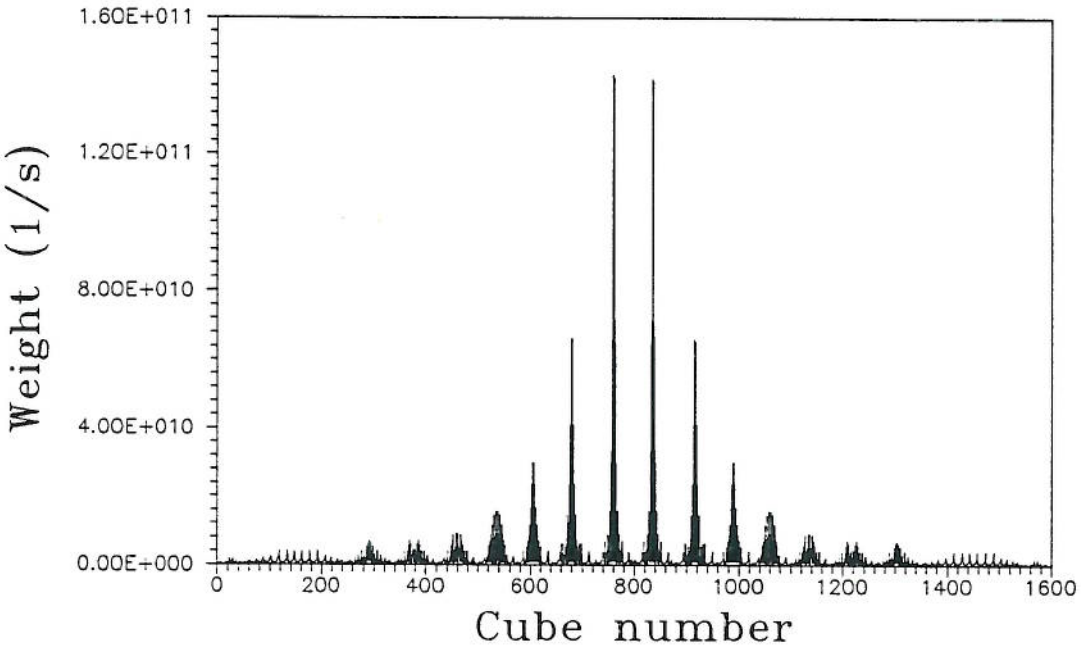

Figure 3.8: Cube weights for $H \rightarrow H$ ionized impurity scattering. Initial state at 0.10 eV on [100] axis.

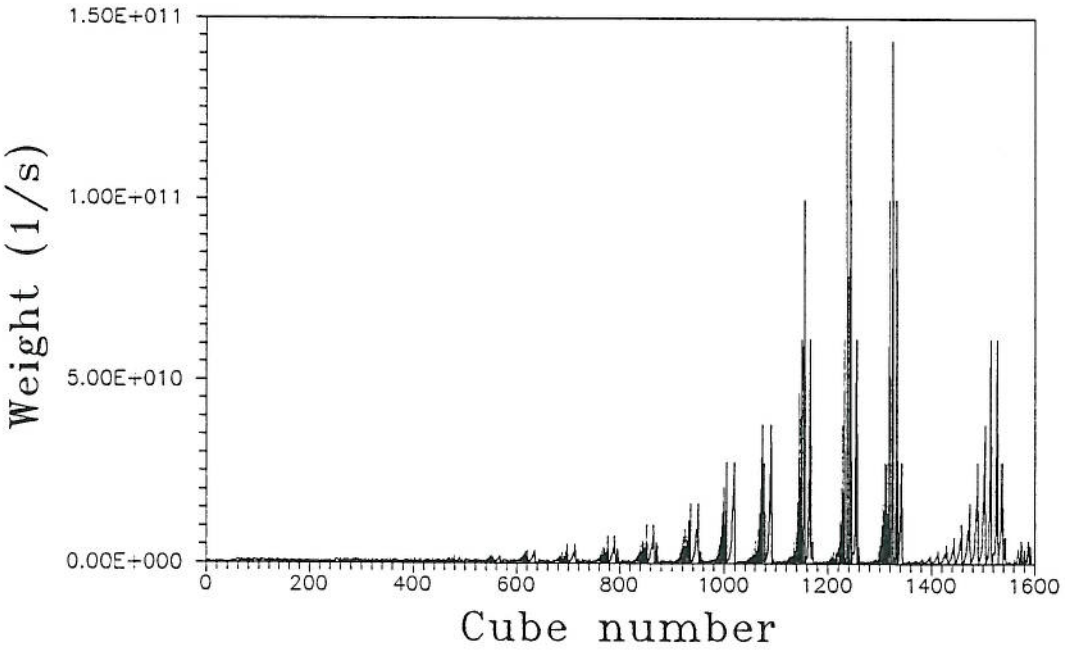

Figure 3.9: Cube weights for $H \rightarrow H$ ionized impurity scattering. Initial state at 0.10 eV on [111] axis.

Figure 3.10 shows the weights for scattering from the light to heavy hole band by ionized impurity scattering. The weights are strongly varying, but far less than for intraband scattering. The rejection method can be expected to perform much better in this case. Regardless

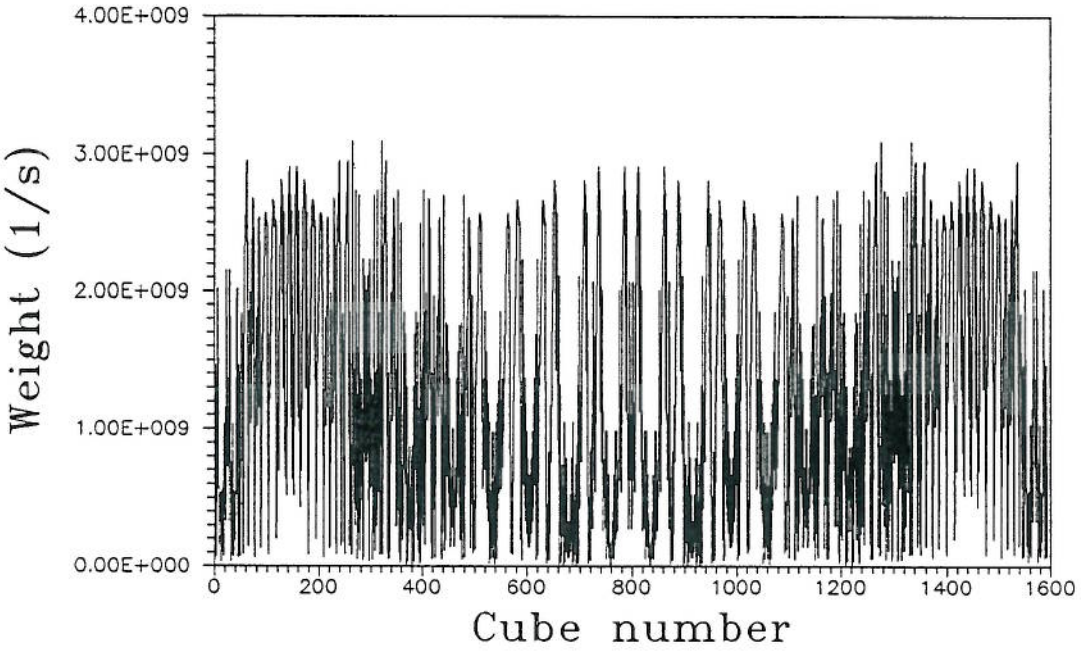

Figure 3.10: Cube weights for $L \rightarrow H$ ionized impurity scattering. Initial state at 0.10 eV on [100] axis.

of how nice the matrix elements behave we must expect a rather "hairy" distribution of weights among the final cubes. The variation is also caused by the different cross-section areas in the different cubes not only by the matrix elements. From this fact alone we can tell that a fully discretized MC simulation will be far more computer demanding than a traditional simulation.

It is not straightforward to give the best possible solution to the problem. For future work several alternatives must be tested against each others. A possible solution is to treat scattering to near cubes and scattering to the other cubes as separate mechanisms. This is a rather artificial approach, but does not alter the physical model. The gain in efficiency should outweigh the disadvantage of complicating the program. Another possible solution is to insert each final cube encountered during the search into an array in a sorted manner. They should be sorted on increasing or decreasing q. Then one could find from the knowledge of the matrix element, an upper bound function for the weights and the combined technique could be used.

Chapter 4

Results and discussion.

In this chapter results from valence band and scattering rate calculations are presented and discussed. The first section deals with the valence band structure of GaAs, and the other with scattering rates in this material. In addition to provide a basis for discussing the rates, the first section also demonstrates the results of first and second derivatives calculations of the dispersion relation. The split-off band is not treated in this chapter because of its insignificant influence on carrier transport in the range of energies investigated. This is due mainly to its very small DOS and that it is split off by a considerable amount of energy (0.34 eV). It is only included in the band calculations as previously described.

4.1 Valence bands of GaAs

For rate calculations the energies, gradients and eigenvectors have been calculated by the program KPBAND. For plotting graphs special programs using the same algorithms have been written. All the curves in this section are generated by these programs.

The band calculations are rather sensitive to changes in the band parameters. This is reasonable from the fact that in the model used here the $\vec{k} \cdot \vec{p}$ calculations for almost all semiconductors of the zincblende and diamond lattice structure are the same except for the parameters. Determination of band parameters is far from trivial, and a lot of different parameter sets appear in the literature [10,15,16,17]. For this diploma thesis the qualitative differences from parabolic results are more important than precise quantitative results. Therefore the parameters already used in the work of wich this diploma thesis is a smaller part, have been chosen. They are given by Lawætz [15] and are theoretically calculated.

When parameters extracted from experimental data are used, one automatically gets some relativistic effects accounted for (k-dependent spin-orbit interaction for instance). This is of little use here because the linear $\vec{k}$ terns in the hamiltonian are neglected. For more reliable quantitative results the parameters should be more carefully chosen. Also linear terms should be included in the $\vec{k} \cdot \vec{p}$ hamiltonian, and the energy range for which the theory is valid could be extended by also including the lowest conduction band in the hamiltonian.

For this work the $\vec{k} \cdot \vec{p}$ theory has been taken for granted, and no attempt has been made to quantify the precision of the model. There is no doubt, however, that it gives a more realistic picture than the parabolic band models used in analytical calculations.

The accuracy of the numerical energy and eigenvector calculations can be considered to be more than sufficient due to the well behaved problem. Also the gradient calculations are unproblematic in this sense. The calculations of the second derivatives are different because the expression contains the difference between the energy of the band in interest and the other bands in the denominator. This might cause trouble when calculations are done for points in $\vec{k}$ space near a degeneracy point. Fortunately this is of little interest when calculations are done for a mesh to be used in MC simulations because the mesh width is big compared to the dimensions for which we can expect trouble. No peculiarities have been observed in the results.

Radial and isoenergy plots of the hole dispersion relations are shown in figures 4.1 and 4.2 respectively. The dashed curves are parabolic bands with effective masses adjusted to fit the DOS at lower energies as described below. Comparison with the work of others can shed some light on the reliability of the results. Isoenergy plots are given by Wiley [10] and by Brennan and Hess [2]. Wiley's heavy hole band shows a stronger warping. This has been checked out and was found to be due to the parameter choice. The shape is qualitatively the same for the energies given. Brennan and Hess have done full zone $\vec{k} \cdot \vec{p}$ calculations. There is qualitative agreement for the $\{100\}$ planes, but the curves for the $\{110\}$ planes show a a somewhat different behaviour at 0.25 and 0.5 eV which is the only relevant energies given. The discrepancies are difficult to explain purely from parameter differences. The simpler approach used in this thesis should be consistent with full zone calculations for lower energies. This suggests that using the 6×6 hamiltonian for energies up to 0.5 eV is to stretch the theory beyond its capability. For future work one should consider including other bands in the hamiltonian, or maybe the perturbation theory should be extended to higher order.

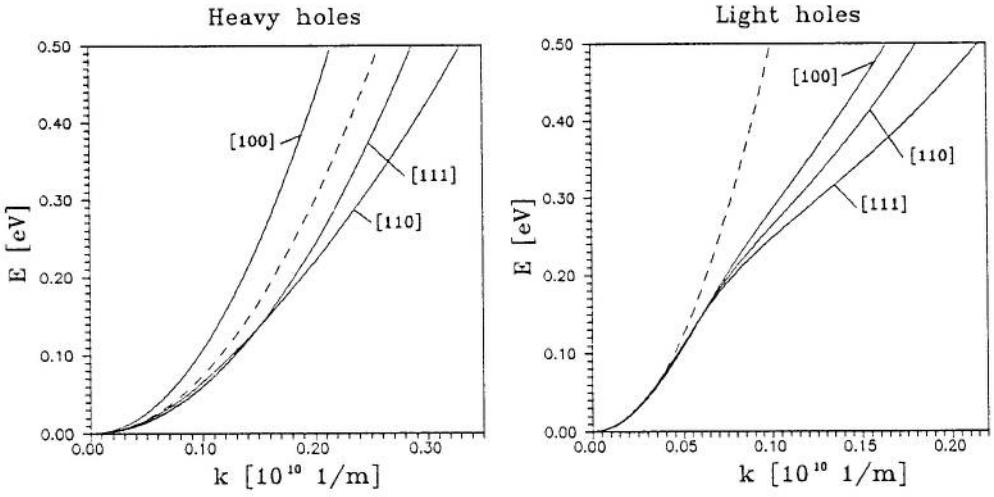

Figure 4.1: Hole dispersion relations in GaAs.

The density of states for the light and heavy hole bands are shown in figure 4.3. They have been calculated by the extrapolation method as described in section 3.2. The dashed line is the DOS for parabolic bands. The effective masses for the parabolic models have been adjusted so that the DOS for the two models coincides at the bottom of the bands. This

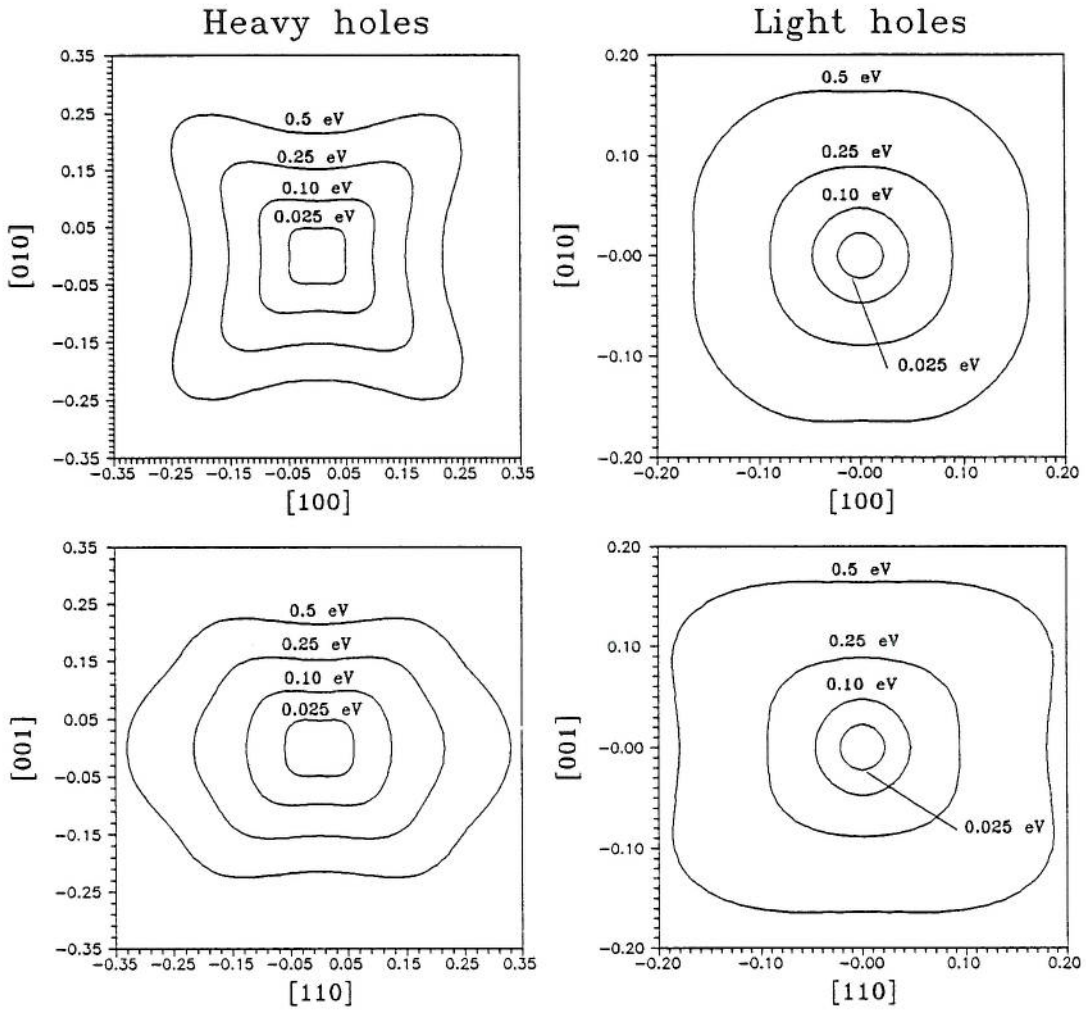

Figure 4.2: Isoenergy plots in two planes. (Units of $10^{10}m^{-1}$)

has been done because there must be some sort of consistence between the two models if the results are to be compared. The adjusted effective masses have been used in the comparison between scattering rates for parabolic and nonparabolic rates in the next section. For the heavy hole band the effective mass is then $0.51m_0$, and for the light hole band it is $0.076m_0$. The effective masses for these two bands used in reference [13] is $0.45m_0$ and $0.082m_0$ respectively. At the time this was written, no information was available on how the latter effective masses were obtained. The discrepancies between the adjusted effective masses and those given in the litterature suggests that the band parameters used in the $\vec{k}\cdot\vec{p}$ calculation should be investigated more carefully for future work.

The figure clearly shows the weakness of the parabolic models also at rather moderate energy levels. Especially in the light hole band the "real" DOS is considerably different from the parabolic. This is due to the characteristic bending of the light hole band giving a considerable deviation from a parabolic band already from approximately 0.10 eV and upwards. The heavy hole band is rather parabolic when plotted along an axis, but the

strong warping has a nonneglible effect on the DOS. The "noise" in the numerical results are due to the extrapolation method, and can be taken as an indication of the accuracy in the calculations. This goes for the scattering rate calculations too. The calculation for the light hole band is more accurate than for the heavy hole band. The reason is that the mesh for the light hole band don't need to cover such an extent of the BZ to contain all the states of energies up to 0.5 eV. Thus a finer mesh is obtained for the light hole band when the numbers of meshpoints are equal.

It is not clearly seen from the figure, but the DOS is not zero at $E = 0$. This is due to the limitations of the extrapolation method.

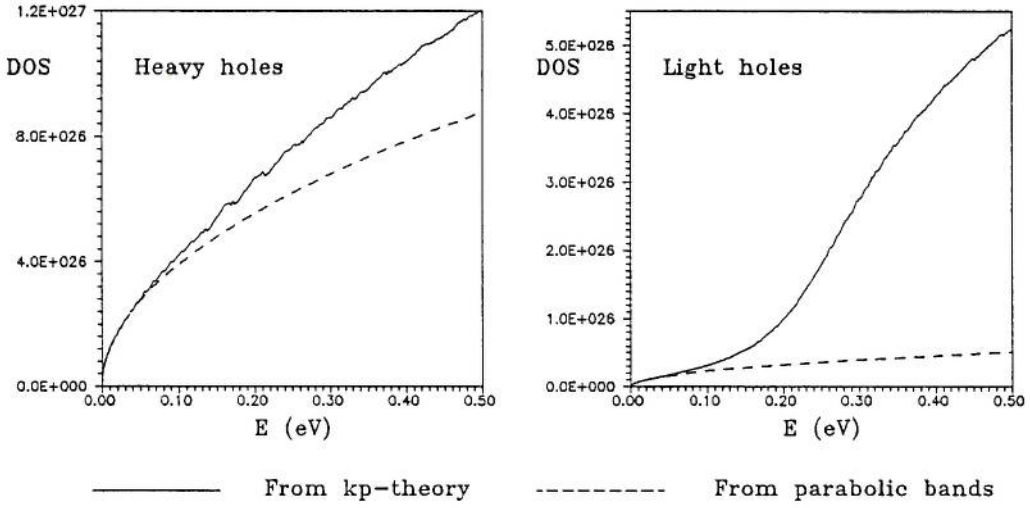

Figure 4.3: Density of states (spin not included).

In figure 4.4 first and second derivatives along different axes are shown. The heavy hole band behaves rather parabolic in the [111] and [100] directions. For the [110] direction a nonparabolic behaviour is seen. The warping is evident from the second derivatives plot. The strong nonparabolicity of the light hole band is shown here as in the radial energy plot (figure 4.1). The second derivatives plot also reveals a weak warping of the light hole band at the bottom. In the [111] and [100] directions the light and heavy hole derivatives approach each other for higher values of the wavevector.

The strange behaviour at $k = 0$ for the second derivatives illustrates the earlier mentioned problem of distingushing the eigenvectors at a point of degeneracy. When the wrong eigenvectors are used the algorithm fails, of course. It is only the points evaluated at $k = 0$ which cause trouble here. That the effect is so clearly visible is due to the spacing between the calculated points. It is not a measure of how close to $k = 0$ the algorithm will work.

4.2 Hole scattering rates in GaAs.

The scattering rate calculations have been performed using a modified version of SCRATES calculating rates for initial states along an axis only. This has been done to save cpu time and to take plots with spacing between the points small enough to reveal errors or inaccuarcies

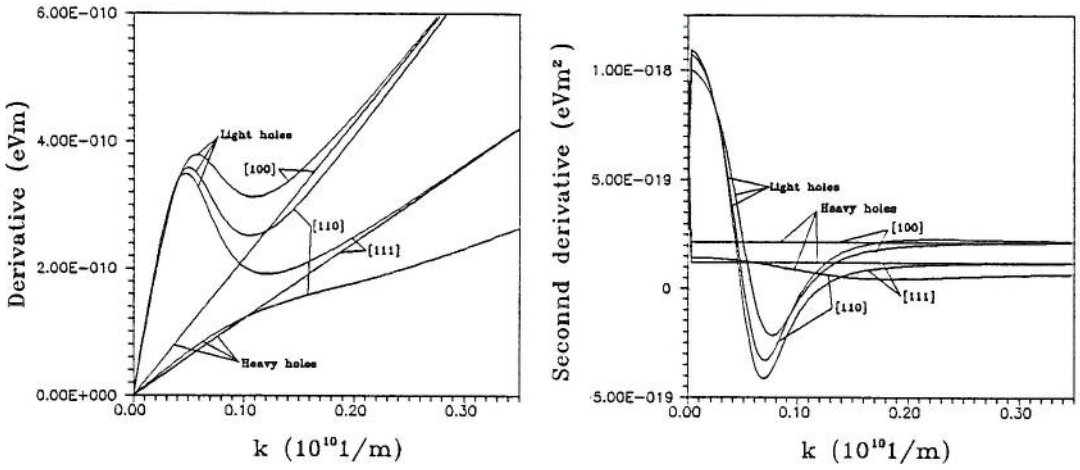

Figure 4.4: Derivatives of energy along different directions.

in the calculations. All the analytical parabolic rates given here have been provided by reference [13].

The physical models have already been mentioned , but deserve some further comments. Overlap integrals are included as multiplicative factors in all calculations except for nonpolar optical scattering. The overlap factors have been calculated from the eigenvectors from $\vec{k} \cdot \vec{p}$ calculations. The results should be considered as one step further from an analytical description using parabolic band models. The improvements lie in the band model and the calculation of overlap factors. There are at least two inconsistencies in the calculation. The matrix element of acoustic deformation potential scattering is originally deducted from 4×4 $\vec{k} \cdot \vec{p}$ theory, but here overlap integrals are calculated from 6×6 theory. The nonpolar optical scattering is also based on a 4×4 approach. (Se the pioneer work on the deformation potential theory by Pikus and Bir [21].) For all mechanisms, bands calculated by 6×6 theory are used. Thus the matrix element of acoustic deformation potential scattering is inconsistently calculated, and the matrix elements used for both deformation potential mechanisms are inconsistent with the band calculations. The matrix elements of the other mechanisms are deducted from more general considerations, and the actual form of the wavefunctions enter in the overlap integral only. The deformation potential scattering mechanisms should be revised in future work, and the inconsistency can perhaps be removed by calculating the entire matrix elements for the deformation potential mechanisms numerically without doing all the approximations necessary to arrive at the analytical matrix elements. The approximations which look best at the time being have been used here.

Scattering rates are given for all the mechanisms in interest for initial states in the [100] direction. In order to demonstrate some anisotropy effects due to the bandstructure, ionized impurity scattering is also given in the [111] direction. All rates are computed for a temperature of 300K. The rates are plotted as function of energy because they are easier to discuss physically from this point of view. The rate calculations have been performed on a VAX8600 in order to handle the big amount of data. The meshes used had 34 meshpoints along an axis. For the heavy holes the coarse mesh had an energy limit of 0.584 eV and

the fine mesh 0.130 eV. The limits for the light hole band where 0.567 eV and 0.259 eV respectively.

In order to shed some light on the weaknesses and strengths of the extrapolation method, some calculations for parabolic band models are shown in figure 4.5. The analytical results are included as dashed curves. The effective masses from [13] have been used here contrary to the other calculations. This is not important for the conclusions, however. The fine meshes cover much lower energies here, 0.054 eV for the heavy hole band and 0.057 eV for the light hole band. The coarse meshes are comparable to those for the nonparabolic rates.

The trouble with the intraband scattering by polar optical phonons and ionized impurities is evident. Though the curves for polar optical phonons are rather ugly, the deviation can be considered acceptable. For intraband ionized impurity scattering the situation is different due to the more nasty behaviour of the matrix element. The worst results are obtained for the heavy hole band, because of the coarser mesh. Because of the strong variation of the matrix elements for small q, the error is heavily dependent on the mesh size. This can also be seen from the nice curve for the heavy hole band at lower energies where a much finer mesh is used. The main trouble is caused by "intracube" scatterings, though near cube scatterings are also significant. If we consider "intracube" scattering alone and consider the amount of 'error" in estimating the average of the squared matrix element approximately the same for the two bands, we have that the errors in the total rates for the two bands will be proportional to the DOS of the cubes. The DOS of the heavy hole band cube will be much greater than that for the light hole band, due to the larger cross-section area (and the smaller gradient). This is of course a simplification of what actually happens, but it explains sufficiently well why the errors are so different.

For the heavy hole band, calculations along the [111] axis are also included. The figure shows that the errors are quite different from the [100] direction. This must be so because when we move along the [100] axis we never move through a meshpoint, so very small q will never be accounted for. In the [111] direction we will encounter meshpoints at distances $2\sqrt{3}b$ in $\vec{k}$-space, and the matrix element will be evaluated for $q = 0$ at these points. This will give an overestimate. Similiarly there are points along this axis displaced by the same amount, for which we will be at a distance $\sqrt{3}b$ from the nearest meshpoints, and the matrix element will be evaluated for $q \approx \sqrt{3}b$, which will give an underestimate. Subsequently we get the oscillatory behaviour shown in figure 4.5a. In fact the peaks are displaced an amount $2\sqrt{3}b$ in k-space. A similiar reasoning holds for the intraband polar optical plots. For the light hole band the [111] direction is not shown.

Figure 4.5a also includes rates for intraband light and heavy hole scattering calculated by averaging the squared matrix elements over the cross-section area. This has been done by the Monte Carlo technique described in section 3.2. The averages are taken over 500 points for the cubes with center closer to the initial k-vector than $4b$. The curve for the heavy hole band is marked "Averaged". For the light hole band it is not marked because it is close to the nonaveraged curve. It is should be noticed that the small peaks in the plot for the light hole band is for the nonaveraged calculation.

The interband ionized impurity plots posess no visible deviation from the analytic result in the curves. Interband scattering does not cause trouble in the same way as intraband scattering because of the overlap factors and the always nonzero q. Interband scattering is suppressed in the forward and backward directions due to the shape of the overlap integrals

(see figure 3.6). Then intra- or near cube scattering is not important. Closer examination of the data shows that the deviation is no worse than 0.5% for these rates. This is indeed very good, but is partially due to the nice behaviour of the parabolic bands. Such a good performance can not be expected for the rates for nonparabolic bands. When averaging is done for intraband ionized impurity scattering, numerical parabolic calculations show that the "noise" in the results can be taken as a measure of the inaccuracy.

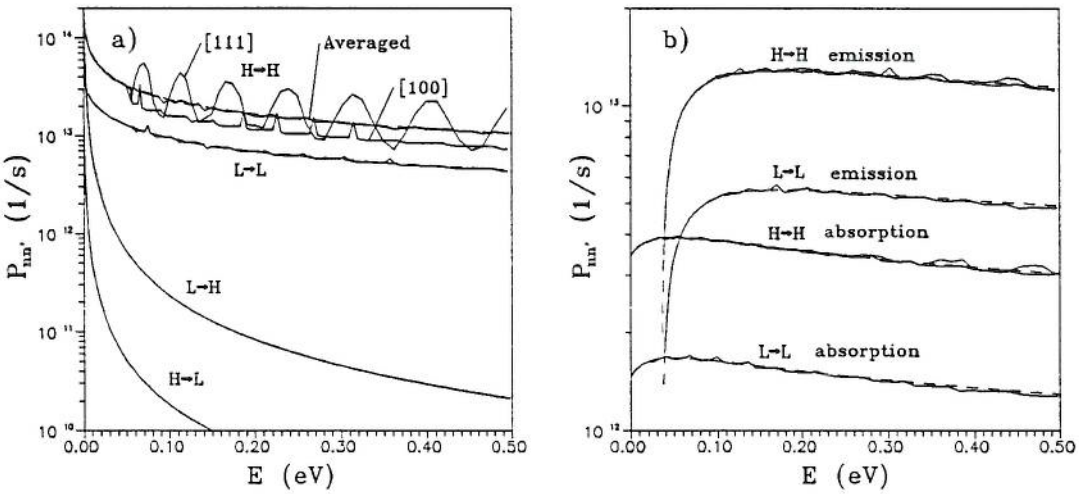

Figure 4.5: a) Ionized impurity scattering. b) Polar optical scattering.

The scattering rates for a nonparabolic bandstructure is shown in figures 4.6-4.8 for initial wavevector in the [100] direction. Intraband ionized impurity scattering has been calculated by the MC averaging method previously described. Analytical results for parabolic bands are shown by dashed curves. They are calculated from the adjusted effective masses.

The behaviour of the scattering rates can be understood in terms of the DOS and the form of the squared matrix elements including the overlap factors. The mechanisms with strong preference for small q scattering can be well understood by introducing the term "local density of states". This means the density of states for a subset of the BZ. The extrapolation method provides some insight to the properties of this term because it is exact in the limit of an infinite mesh. For a cube the extrapolation method gives a DOS inverse proportional to the gradient at the cube center. The gradient of the dispersion relation at a point will then be a measure of the local DOS in a region around this point. At regions of the BZ where the gradient of the light and heavy hole band are approximately equal in magnitude, the scattering rates for the mechanisms with strong preference for small q scattering will be the same order of magnitude for $L \rightarrow L$ and $H \rightarrow H$ transitions. This is clearly shown in the scattering rates for intraband ionized impurity and polar optical scattering in figure 4.6a and 4.7 where the scattering rates for higher energies are not very dependent on the band.

The $H \rightarrow H$ transitions for these two mechanisms in general show a smaller magnitude than the parabolic rates. This is due to the fact that the dispersion relation is steeper than the parabolic band along this axis. Thus the local density of states is smaller than for a

parabolic band. The exception is polar optical emission. Here we see that the rate is higher in the lower energy regime and crosses the parabolic rate somewhere below 0.3 eV. This happens because the effect of a smaller DOS is outweighted by the higher contribution from small q scattering for scattering to the lower energies.

For $L \rightarrow L$ transitions we have that the rates are in general higher than the parabolic results. This must be explained by the higher DOS. The differences between the parabolic and nonparabolic rates for scattering to the light hole band are for all rates dominated by the much higher DOS for the nonparabolic band. For ionized impurities the $L \rightarrow L$ scattering rate goes nicely to the parabolic result for small energies as expected from the DOS and dispersion relation plots.

The nonpolar optical scattering (fig.4.6b)is a rather straightforward mechanism to calculate due to the constant matrix element used in this model. The shapes of the rates are only dependent on the final band. The rates approach the analytical parabolic results at lower energies. The rates are proportional to the DOS of the final band at the final energy. Thus it is seen that the heavy hole rate is about 30% higher than the parabolic rate at 0.5 eV. The light hole rates also increase with energy according to the DOS and reach values about half of the corresponding heavy hole rate. This is also consistent with the DOS. The irregularities in the heavy hole curves are due to the extrapolation method and can also be seen in the DOS plot. It can also be seen that the peaks in the irregularities for the two curves are displaced approximately $2\hbar\omega_0 = 0.07eV$.

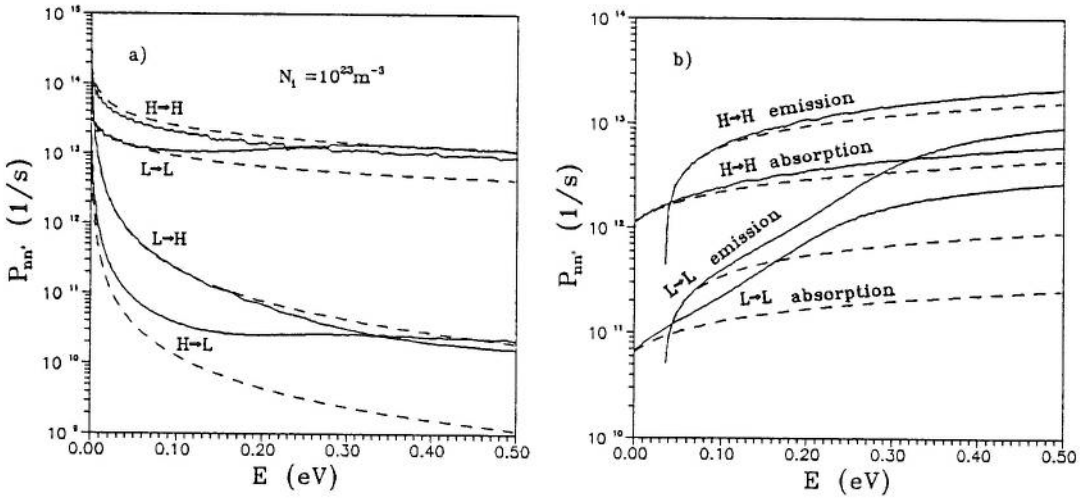

Figure 4.6: a) Ionized impurity scattering. b) Nonpolar optical scattering.

Figure 4.8 shows the scattering rates for acoustic deformation potential scattering. Some of the curves are by a mistake not calculated all the way up to 0.5 eV, but the tendency is clear. The matrix element of this mechanism is rather well behaved. The angular dependence of the scattering is mainly determined by the overlap factors. Thus near forward/backward scattering will dominate the intraband scattering somewhat and be suppressed for interband scattering. Neither the equipartion nor the elastic approximation have been used. Inelastic scattering has been taken into account by using the cube centres to evaluate ΔE^m. The small variations in the rates are mainly due to the extrapolation

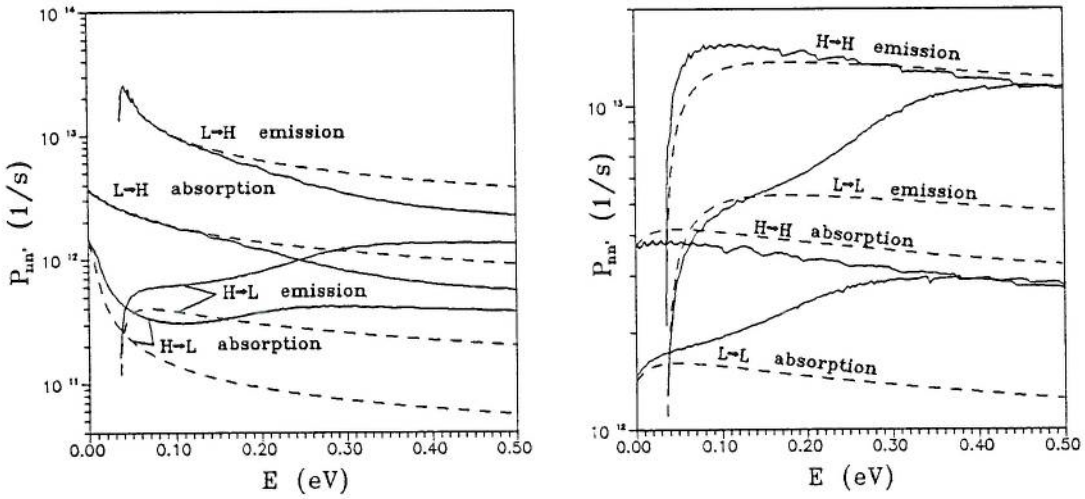

Figure 4.7: Polar optical scattering.

method as seen for the nonpolar optical scattering.

The effect of the higher DOS is clearly shown for scattering to the light hole band as for the other mechanisms. Also all the rates approximately approaches the parabolic result for lower energies. For heavy hole intraband scattering the scattering rates are clearly lifted compared to the parabolic results. For light to heavy hole scattering the situation is opposite. The intraband effects are explained by the higher DOS because the overlap factors are very similiar to the analytical model. For interband scattering we have that the overlap factors decrease with higher energies causing a smaller scattering rate than the analytical result which have overlap factors only dependent on the scattering angles. This tendency can be seen for most interband scatterings. It is not quite clear from the figure,

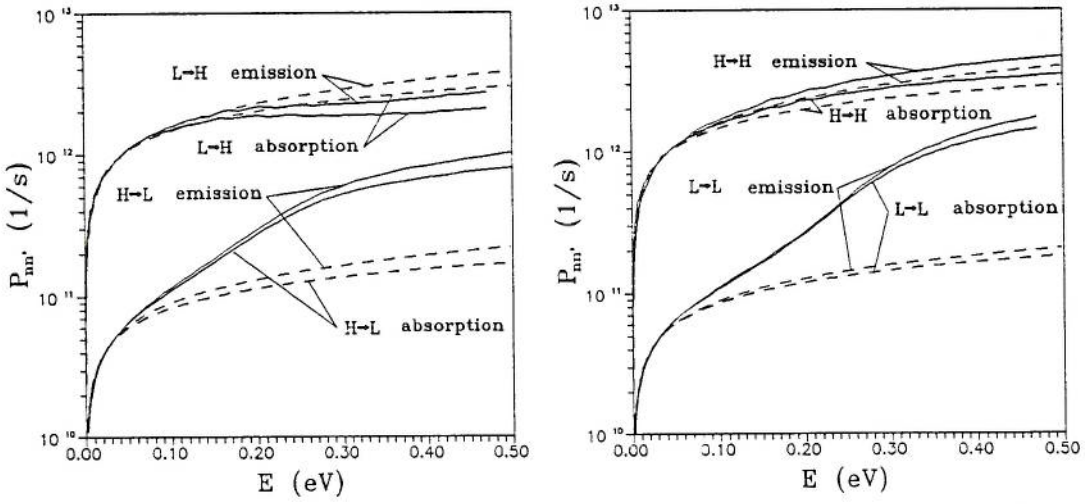

Figure 4.8: Acoustic deformation potential scattering.

but there is for all transitions an energy where the emission and absorption rates cross.

This is also the case for the analytical parabolic results.

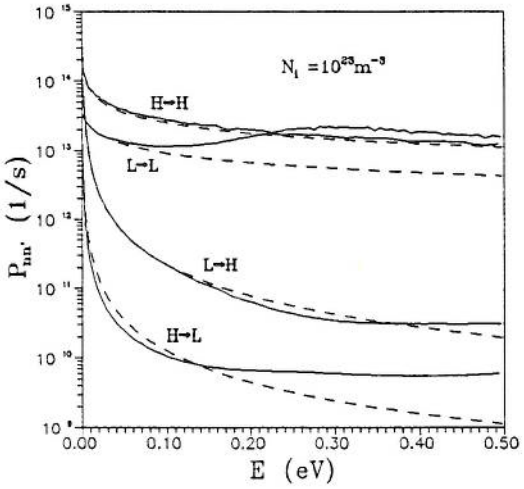

Figure 4.9: Ionized impurity scattering. (Initial $\vec{k}$ along [111])

Figure 4.9 shows ionized impurity scattering for initial $\vec{k}$ along the [111] direction. For intraband scattering we see that the rates are clearly lifted compared to the [100] direction and that they are above the parabolic results. This is due to the higher local DOS along this axis. The heavy to light hole scattering shows the most pronounced differences from the [100] direction.

It is appropriate to give some general remarks about the interband scattering for ionized impurities and polar optical phonons. The matrix elements excluding overlap factors for these mechanisms have a strong preference for small q scattering. The overlap factor for the interband scattering will have the opposite effect because it strongly suppresses the forward scattering. Thus we have to strong effects which work opposite of each other. The complicated bandstructure and the $\vec{k}$ dependence of the overlap factor obscures the picture even more. It is therefore not safe to draw any solid conclusions on what causes the shapes of the rates.

The software has been thoroughly tested against known data for analytical parabolic bands and no peculiarities have been observed provided the averaging is done for intraband ionized impurity scattering. All results obtained indicates that the "noise" in the plots and the DOS gives a good estimate of the error in the rate. From investigation of the plots this indicates an error of about $\pm 10\%$ for all rates except ionized impurity scattering which has at least the double in the worst case. Some rates behave better than this, especially those with final states in the light hole band, but the number reflects the general tendency. The error estimate can be expected to fail for scattering to states near $\vec{k} = 0$.

It is a general trend in the curves that the difference between $H \rightarrow L$ and $L \rightarrow H$ transitions are less than for the analytical parabolic rates. Thus we should expect that the nonparabolic rates will give higher population of the light hole band and lower population of the heavy hole band under stationary conditions than the parabolic results. Also we can expect a considerable anisotropy of the polar optical scattering rate just as for ionized impurity scattering. The nonpolar rate is isotropic. The acoustic deformation potential

scattering can be expected to show a much weaker anisotropy than the ionized impurity scattering. To figure out how all this will affect charge transport we need to do a MC simulation.

Chapter 5

Summary and conclusions.

A program has been developed to calculate the valence band and related quantities for GaAs. Equations have been found which make it possible to calculate the derivatives of the dispersion relation within machine precision if the eigenvalues and eigenvectors are known with such precision. The algorithms used in the program will be usefull regardless of the level of sophistication of the $\vec{k} \cdot \vec{p}$ theory used.

A program for calculating scattering rates in GaAs has been written. The algorithm originally used by Fischetti and Laux needed a slight modification to avoid problems with intraband ionized impurity and polar optical scattering. The Monte Carlo averaging procedure which has been used here is adequate for rate plots, but must be replaced by analytical equations in future programs.

The final cube weights have been investigated to see what to expect when a Monte Carlo analysis will be done. It is clear from the examples that special care must be taken to reduce the number of rejections. This will be very critical in a final MC program. The amount of data needed in a discretized MC program also gives an indication of how big the task is.

Scattering rates have been calculated for GaAs using the two programs. The error in the results are estimated to be within 10% for all mechanisms except ionized impurity scattering. The lack of precision must be considered an intrinsic property of the extrapolation method. It is the price we must pay for the discretization. The errors are however strongly dependent on the mesh size, and much can be accomplished by finding good ways of estimating the averages of the scattering matrix element. The errors are small compared to the effects of the bandstructure so the rates obtained should give a reliable picture of the differences from analytical parabolic rates.

The calculations show a clear increase in the heavy to light hole scattering compared to the light to heavy hole scattering. Thus we might expect a shift in the carrier population of the two bands compared to analytical results. Anisotropic scattering rates for ionized impurity scattering has been demonstrated. Similiar effects can be expected for polar optical scattering.

Appendix A

Derivatives of energy and overlap factors

For interpolation purposes and to find the carrier group velocity, we need to know the gradient and the second derivatives of the dispersion relation. When the band structure is found from $\vec{k} \cdot \vec{p}$ theory, the hamiltonian is represented as a complex hermitian matrix (6x6 in this work). Each entry in the matrix is a known function of the wavevector, $\vec{k}$. For each point calculated in the dispersion relation the eigenvectors are also calculated. This is all that is needed to find the derivatives at a specific point in k-space. $E(\vec{k})$ is found by solving the eigenproblem (A.1) for each value of $\vec{k}$.

$$\mathcal{H}\mathcal{F} = E\mathcal{F} \tag{A.1}$$

Here $\mathcal{H}$ is the $\vec{k} \cdot \vec{p}$ hamiltonian, E is the energy and $\mathcal{F}$ is the corresponding eigenvector written as a column matrix. The deductions are based on the following conditions:

- $\mathcal{H}$ is a complex hermitian matrix.
- $\mathcal{H}$,E and $\mathcal{F}$ are differenciable with respect to any component of the wavevector.
- $\mathcal{F}$ and E are given by equation (A.1). Then the different eigenvectors for a given $\vec{k}$ are orthogonal or may be chosen to be orthogonal. They can be nomalized to unity. Thus we have a complete set of orthonormal eigenvectors for each $\vec{k}$. Because $\mathcal{H}$ is complex hermitian all the eigenvalues are real.

A.1 First derivatives

The specific solution for band n and wave vector $\vec{k}$ obeys equation (A.1). Suppressing the wavevector dependence in the notation we write:

$$\mathcal{H}\mathcal{F}_n = E_n\mathcal{F}_n \tag{A.2}$$

We seek the energy derivative with respect to k_α by differenciating this equation. The subscript, α, means that k_α represent either the x,y or z component of the wavevector.

$$\mathcal{H}_\alpha \mathcal{F}_n + \mathcal{H}\frac{\partial}{\partial k_\alpha}\mathcal{F}_n = \frac{\partial E_n}{\partial k_\alpha}\mathcal{F}_n + E_n\frac{\partial}{\partial k_\alpha}\mathcal{F}_n \tag{A.3}$$

The matrix $\mathcal{H}_\alpha$ is the derivative of $\mathcal{H}$ with respect to k_α. It is hermitian when $\mathcal{H}$ is. Then we multiply from left by the conjugate transpose (denoted by $^+$) of the eigenvector and use the fact that $\mathcal{H}$ is hermitian to obtain an expression for the derivative:

$$\frac{\partial E_n}{\partial k_\alpha} = \mathcal{F}_n^+ \mathcal{H}_\alpha \mathcal{F}_n \tag{A.4}$$

A.2 Second derivatives

We use a similiar approach for the second derivatives, but we take the derivative of equation (A.3) with respect to k_β ($\beta = x,y$ or z). With $\mathcal{H}_{\alpha\beta} = \frac{\partial^2 \mathcal{H}}{\partial k_\alpha \partial k_\beta}$ we get :

$$\begin{aligned}
&\mathcal{H}_{\alpha\beta}\mathcal{F}_n + \mathcal{H}_\alpha\frac{\partial}{\partial k_\beta}\mathcal{F}_n + \mathcal{H}_\beta\frac{\partial}{\partial k_\alpha}\mathcal{F}_n + \mathcal{H}\frac{\partial^2}{\partial k_\alpha \partial k_\beta}\mathcal{F}_n \\
&= \frac{\partial^2 E_n}{\partial k_\alpha \partial k_\beta}\mathcal{F}_n + \frac{\partial E_n}{\partial k_\alpha}\frac{\partial}{\partial k_\beta}\mathcal{F}_n + \frac{\partial E_n}{\partial k_\beta}\frac{\partial}{\partial k_\alpha}\mathcal{F}_n + E_n\frac{\partial^2}{\partial k_\alpha \partial k_\beta}\mathcal{F}_n
\end{aligned} \tag{A.5}$$

We may write the first derivative of the eigenvector as a linear combination of all the eigenvectors because they form a complete set in our finite dimensional vector space:

$$\frac{\partial}{\partial k_\alpha}\mathcal{F}_n = \sum_i d_{ni}^\alpha \mathcal{F}_i \tag{A.6}$$

The coefficients in the sum term are complex and dependent on $\vec{k}$. From the orthonormality and the equation above we find that

$$d_{ni}^\alpha = -d_{in}^{\alpha\,*} \tag{A.7}$$

$$\Re e\{d_{nn}^\alpha\} = 0 \tag{A.8}$$

If equation (A.6) is inserted in (A.5), a multiplication from left by $\mathcal{F}_n^+$ will give us the following expression for the second derivative:

$$\frac{\partial^2 E_n}{\partial k_\alpha \partial k_\beta} = \mathcal{F}_n^+ \mathcal{H}_{\alpha\beta}\mathcal{F}_n + \sum_{i\neq n} d_{ni}^\beta \mathcal{F}_n^+ \mathcal{H}_\alpha \mathcal{F}_i + \sum_{i\neq n} d_{ni}^\alpha \mathcal{F}_n^+ \mathcal{H}_\beta \mathcal{F}_i \tag{A.9}$$

The remaining task is to determine the unknown coefficents. We insert the linear combination (A.6) into equation (A.3) and multiply from left by $\mathcal{F}_j^+$ letting j denote an arbitrary eigenvector.

$$\mathcal{H}_\alpha \mathcal{F}_n + \sum_i d_{ni}^\alpha E_i \mathcal{F}_i = \frac{\partial E_n}{\partial k_\alpha}\mathcal{F}_n + E_n \sum_i d_{ni}^\alpha \mathcal{F}_i \tag{A.10}$$

$$\mathcal{F}_j^+ \mathcal{H}_\alpha \mathcal{F}_n + E_j d_{nj}^\alpha = \frac{\partial E_n}{\partial k_\alpha}\delta_{nj} + E_n d_{nj}^\alpha \tag{A.11}$$

For $i \neq n$ we get :

$$\mathcal{F}_i^+ \mathcal{H}_\alpha \mathcal{F}_n = d_{ni}^\alpha (E_n - E_i) \tag{A.12}$$

Equation (A.12) tells us that all summation terms in (A.9) disappears for $E_i = E_n$. Thus we have an expression for all the coefficients of the terms that don't vanish. Using this and the property $d_{ni}^\alpha = -d_{in}^{\alpha\,*}$, we may now write the second derivative as :

$$\frac{\partial^2 E_n}{\partial k_\alpha \partial k_\beta} = \mathcal{F}_n^+ \mathcal{H}_{\alpha\beta} \mathcal{F}_n + 2 \sum_{\substack{i \\ E_i \neq E_n}} \frac{\Re e \left\{ (\mathcal{F}_i^+ \mathcal{H}_\beta \mathcal{F}_n)(\mathcal{F}_n^+ \mathcal{H}_\alpha \mathcal{F}_i) \right\}}{E_n - E_i} \tag{A.13}$$

A.3 Derivative of overlap factors.

The intention here is to find an expression from which we can calculate the derivative of the overlap factors. We do this by first finding:

$$\frac{\partial}{\partial k_\alpha} \left| \mathcal{F}^+_{m\vec{k}'} \mathcal{F}_{n\vec{k}} \right|^2 = 2\Re e \{ \mathcal{F}^+_{m\vec{k}'} \mathcal{F}_{n\vec{k}} \frac{\partial}{\partial k_\alpha} \mathcal{F}^+_{m\vec{k}'} \mathcal{F}_{n\vec{k}} \} \tag{A.14}$$

Here k_α denotes a component of the initial wavevector $\vec{k}$. By writing the derivative as a linear combination of all the eigenvectors as before and using equation (A.12) we get

$$\frac{\partial}{\partial k_\alpha} \mathcal{F}_{n\vec{k}} = \sum_{\substack{i \\ E_i \neq E_n}} \frac{\mathcal{F}^+_{i\vec{k}} \mathcal{H}_\alpha \mathcal{F}_{n\vec{k}}}{E_n - E_i} + \sum_{\substack{i \\ E_i = E_n}} d_{in}^\alpha \mathcal{F}_{i\vec{k}} \tag{A.15}$$

Now we will restrict our attention to doubly degenerate bands. The approch is similiar for higher degeneracies. We denote the state degenerate with $\mathcal{F}_{n\vec{k}}$ by $\mathcal{F}_{n'\vec{k}}$. Equation (A.14) can now be written on the form:

$$\begin{aligned} \frac{\partial}{\partial k_\alpha} \left| \mathcal{F}^+_{m\vec{k}'} \mathcal{F}_{n\vec{k}} \right|^2 &= 2\Re e \left\{ (\mathcal{F}^+_{m\vec{k}'} \mathcal{F}_{n\vec{k}})^* \sum_{\substack{i \\ E_i \neq E_n}} \frac{\mathcal{F}^+_{i\vec{k}} \mathcal{H}_\alpha \mathcal{F}_{n\vec{k}}}{E_n - E_i} \mathcal{F}^+_{m\vec{k}'} \mathcal{F}_{i\vec{k}} \right\} \\ &+ 2\Re e \left\{ d_{n'n} (\mathcal{F}^+_{m\vec{k}'} \mathcal{F}_{n\vec{k}})^* \mathcal{F}^+_{m\vec{k}'} \mathcal{F}_{n'\vec{k}} \right\} \end{aligned} \tag{A.16}$$

Now adding the similiar equation for $|\mathcal{F}^+_{m\vec{k}'} \mathcal{F}_{n'\vec{k}}|^2$ and using (A.7) we obtain an expression which is directly applicable to finding the derivative of the overlap factor:

$$\begin{aligned} &\frac{\partial}{\partial k_\alpha} \left(|\mathcal{F}^+_{m,\vec{k}'} \mathcal{F}_{n,\vec{k}}|^2 + |\mathcal{F}^+_{m,\vec{k}'} \mathcal{F}_{n',\vec{k}}|^2 \right) = \\ &\quad 2\Re e \left\{ (\mathcal{F}^+_{m,\vec{k}'} \mathcal{F}_{n,\vec{k}})^* \sum_{\substack{i \\ E_i \neq E_n}} \frac{\mathcal{F}^+_{i,\vec{k}} \mathcal{H}_\alpha \mathcal{F}_{n,\vec{k}}}{E_n - E_i} \mathcal{F}^+_{m,\vec{k}'} \mathcal{F}_{i,\vec{k}} \right\} \\ + \quad &2\Re e \left\{ (\mathcal{F}^+_{m,\vec{k}'} \mathcal{F}_{n',\vec{k}})^* \sum_{\substack{i \\ E_i \neq E_n}} \frac{\mathcal{F}^+_{i,\vec{k}} \mathcal{H}_\alpha \mathcal{F}_{n',\vec{k}}}{E_n - E_i} \mathcal{F}^+_{m,\vec{k}'} \mathcal{F}_{i,\vec{k}} \right\} \end{aligned} \tag{A.17}$$

Appendix B

Physical constants and material parameters

Here the physical constants and material parameters used in the programs are given. Their symbols, values and program variable names are listed together with a brief explanation of what they represent. All material parameters are from [13] except the band parameters included the spin-orbit splitting [15].

Physical constants			
Symbol	Value	Variable	Explanation
$\hbar$	$1.05459 \cdot 10^{-34} Js$	HBAR	Plancks constant $/2\pi$
ϵ_0	$8.8542 \cdot 10^{-12} C^2/Nm^2$	EPSO	Vacuum dielectric constant
e	$1.60219 \cdot 10^{-19} C$	EC	Elementary charge
k_B	$1.3807 \cdot 10^{-23} J/K$	KB	Boltzmann's constant

Material parameters for GaAs			
Symbol	Value	Variable	Explanation
ϵ_∞	10.92	EPSINF	High frequency relative dielectric permittivity
ϵ_s	12.9	EPSZER	Static relative dielectric permittivity
$\hbar\omega_0$	$0.035eV$	OPTEN	Optical phonon energy
E_1	$5.6eV$	D	Acoustic deformation potential
$\bar{s}$	$3860m/s$	S	Average velocity of sound
ρ	$5360kg/m^3$	RHO	Mass density
$(DK)^2$	$1.58 \cdot 10^{22} eV^2/m^2$	DKSQR	Optical phonon coupling constant
N_i	–	NIMP	Ionized impurity concentration
a	$3.1eV$	AS	Deformation potential
b	$-1.7eV$	BS	Deformation potential
d	$-4.4eV$	DS	Deformation potential
A	-7.98	A	Band parameter (units of $\frac{\hbar^2}{2m}$)
B	-5.16	B	Band parameter (units of $\frac{\hbar^2}{2m}$)
D	-11.09	D	Band parameter (units of $\frac{\hbar^2}{2m}$)
Δ	$0.34eV$	DELTA	Spin orbit splitting.

Appendix C

Squared matrix elements

Here the squared matrix elements are listed. The overlap factors should be multiplied to all of them except for nonpolar optical phonon scattering. For this mechanism the overlap should not be a multiplicative factor. The expression here is the same as that for electrons except for a factor $\frac{1}{2}$. Screening is taken into account for ionzed impurity scattering only. These are the matrix elements used by reference [13].

- Polar optical phonon scattering:

$$|M(q)|^2 = \left\{ \begin{matrix} N(\vec{q}) \\ N(\vec{q}) + 1 \end{matrix} \right\} \frac{e^2 \hbar \omega_0}{2\epsilon_0} \left(\frac{1}{\epsilon_\infty} - \frac{1}{\epsilon_s} \right) \frac{1}{q^2} \tag{C.1}$$

- Acoustic deformation potential phonon scattering:

$$|M(q)|^2 = \left\{ \begin{matrix} N(\vec{q}) \\ N(\vec{q}) + 1 \end{matrix} \right\} \frac{E_1^2 \hbar}{2\rho \bar{s}} q \tag{C.2}$$

- Nonpolar optical phonon scattering:

$$|M(q)|^2 = \left\{ \begin{matrix} N(\vec{q}) \\ N(\vec{q}) + 1 \end{matrix} \right\} \frac{(DK)^2 \hbar}{4\rho\omega_0} \tag{C.3}$$

- Ionized impurity scattering:

$$|M(q)|^2 = \frac{N_i e^4}{\epsilon_0^2 \epsilon_s^2} \frac{1}{(q^2 + \beta^2)^2} \tag{C.4}$$

$$\beta = \left(\frac{N_i e^2}{k_B T \epsilon_0 \epsilon_s} \right)^{\frac{1}{2}} \tag{C.5}$$

The quantity $N(\vec{q})$ is the phonon occupation number:

$$N(\vec{q}) = \frac{1}{\exp\left(\frac{\hbar\omega(\vec{q})}{k_B T}\right) - 1} \tag{C.6}$$

The phonon system is assumed to be in thermal equilibrium. The dispersion relation for acoustic phonons is approximated by $\omega(\vec{q}) = \bar{s}q$. For optical phonons we write $\omega(\vec{q}) = \omega_0$.

Appendix D

Vertices of cross-section area

The vertices of the cross-section area are listed here. They are given as vectors from the cube centre and listed such that the vector for a point appears between the vectors for its nearest neighbouring points.

$w \in [0, w_1]$ and $l_1 \geq l_2 + l_3$:

$$\begin{aligned}
\vec{P}_1 &= b[\frac{1}{l_1}(\frac{w}{b} + l_2 + l_3), -1, -1] \\
\vec{P}_2 &= b[\frac{1}{l_1}(\frac{w}{b} - l_2 + l_3), 1, -1] \\
\vec{P}_3 &= b[\frac{1}{l_1}(\frac{w}{b} - l_2 - l_3), 1, 1] \\
\vec{P}_4 &= b[\frac{1}{l_1}(\frac{w}{b} + l_2 - l_3), -1, 1]
\end{aligned} \tag{D.1}$$

$w \in [0, w_1]$ and $l_1 < l_2 + l_3$:

$$\begin{aligned}
\vec{P}_1 &= b[\frac{1}{l_1}(\frac{w}{b} + l_2 - l_3), -1, 1] \\
\vec{P}_2 &= b[1, -1, \frac{1}{l_3}(\frac{w}{b} - l_1 + l_2)] \\
\vec{P}_3 &= b[1, \frac{1}{l_2}(\frac{w}{b} - l_1 + l_3), -1] \\
\vec{P}_4 &= b[\frac{1}{l_1}(\frac{w}{b} - l_2 + l_3), 1, -1] \\
\vec{P}_5 &= b[-1, 1, \frac{1}{l_3}(\frac{w}{b} + l_1 - l_2)] \\
\vec{P}_6 &= b[-1, \frac{1}{l_2}(\frac{w}{b} + l_1 - l_3), 1]
\end{aligned} \tag{D.2}$$

$w \in [w_1, w_2]$:

$$\vec{P}_1 = b[\frac{1}{l_1}(\frac{w}{b} + l_2 - l_3), -1, 1]$$

$$
\begin{aligned}
\vec{P}_2 &= b[1, -1, \frac{1}{l_3}(\frac{w}{b} - l_1 + l_2)] \\
\vec{P}_3 &= b[1, \frac{1}{l_2}(\frac{w}{b} - l_1 + l_3), -1] \\
\vec{P}_4 &= b[\frac{1}{l_1}(\frac{w}{b} - l_2 + l_3), 1, -1] \\
\vec{P}_5 &= b[\frac{1}{l_1}(\frac{w}{b} - l_2 - l_3), 1, 1]
\end{aligned}
\tag{D.3}
$$

$w \in [w_2, w_3]$:

$$
\begin{aligned}
\vec{P}_1 &= b[\frac{1}{l_1}(\frac{w}{b} - l_2 + l_3), 1, -1] \\
\vec{P}_2 &= b[\frac{1}{l_1}(\frac{w}{b} - l_2 - l_3), 1, 1] \\
\vec{P}_3 &= b[1, \frac{1}{l_2}(\frac{w}{b} - l_1 - l_3), 1] \\
\vec{P}_4 &= b[1, \frac{1}{l_2}(\frac{w}{b} - l_1 + l_3), -1]
\end{aligned}
\tag{D.4}
$$

$w \in [w_3, w_4]$:

$$
\begin{aligned}
\vec{P}_1 &= b[\frac{1}{l_1}(\frac{w}{b} - l_2 - l_3), 1, 1] \\
\vec{P}_2 &= b[1, \frac{1}{l_2}(\frac{w}{b} - l_1 - l_3), 1] \\
\vec{P}_3 &= b[1, 1, \frac{1}{l_3}(\frac{w}{b} - l_1 - l_2)]
\end{aligned}
\tag{D.5}
$$

Appendix E

Program user guides.

E.1 KPBAND user guide.

KPBAND is a program for calculation of the valence band of GaAs for energies not far from the band edge. The program handles semiconductor under homogenous strain. It is based on the $\vec{k} \cdot \vec{p}$-method. The eigenproblem for a 6x6 Kohn-Luttinger hamiltonian is solved. The program calculates:

- Energies
- Energy gradients
- Energy second derivatives
- Eigenvectors

The values are computed for a uniform mesh in k-space. There is an option for creating a finer mesh around $\vec{k} = 0$. For each energy mesh the program also calculates the largest energy which is entirely enclosed by the mesh. The energy span of each cube is found by first order extrapolation. In order to make the program easy to run as a batch job, no keyboard input is required for KPBAND. Instead all user definable parameters are set in a separate program called KPINI. The parameters are stored on a file, "KPBAND.INI", which is read by the program just after start up. The following sections describe how to set up KPBAND and run it. A section on the file formats used is also included.

E.1.1 How to set up KPBAND.

There are a number of parameters which may be set by the user. They are:

- Strain tensor
- Mesh specifications
- Output filenames
- Which bands to calculate

- What to calculate

All these parameters are set from the program KPINI. This program reads the file "KPBAND.INI" and lets the user change its contents. If the file isn't found, or if it can't be read for some reason, a new file by this name is created. The user interface is a simple "no nonsense" menu system. You enter and exit through the main menu. It has the following appearance on the computer screen:

```
**** KPINI MAIN MENU *****

1. Set strain tensor.
2. Describe mesh(es).
3. Set which bands to calculate.
4. Set what to calculate.
5. Define filenames.
6. Show all data.
7. Save and quit

ENTER SELECTION :
```

You choose from the menu by typing the number in front of the menu entry in interest. You always return to the main menu when you finish one of the submenues, except for selection number 7, of course. The selections are described one by one below. User input is shown enclosed in < > in order to distinguish it from program output.

Selection 1: SET STRAIN TENSOR

The user may specify a homogenous strain. It is a second order symmetric tensor. The program shows the current strain on the screen and asks for new values. When they are typed in you return to the main menu immediately:

```
**** SET STRAIN TENSOR ****

Strain:        .0000000    .0000000    .0000000
               .0000000    .0000000    .0000000
               .0000000    .0000000    .0000000

SPECIFY NEW STRAIN (EXX,EXY,EXZ,EYY,EYZ,EZZ):
<0,0,0,0,0,0><ENTER>
```

Selection 2: DESCRIBE MESH(ES)

The program must know for which values of the wavevector the calculations should be done. This information is given to the program by specifying the mesh(es) in $\vec{k}$-space. For each mesh you specify the number of meshpoints and the largest possible wavevector component along an axis. The latter is given as a fraction of $\frac{2\pi}{a_0}$, where a_0 is the lattice constant. Wether a fine mesh should be created or not is optional. The example below shows how the meshes are described in the program.

```
**** DESCRIBE MESH(ES) ****
Coarse mesh:
   1. Number of meshpoints :   2
   2. Fraction of 2*PI/A0  : 1.000

Fine mesh:
   3. No fine mesh is generated.

ENTER SELECTION (0=EXIT) :
<3><ENTER>

**** DESCRIBE MESH(ES) ****
Coarse mesh:
   1. Number of meshpoints :   2
   2. Fraction of 2*PI/A0  : 1.000

Fine mesh:
   3. Fine mesh is generated.
   4. Number of meshpoints :   2
   5. Fraction of 2*PI/A0  : 1.000

ENTER SELECTION (0=EXIT) :
<1><ENTER>

Enter number of meshpoints :
<32><ENTER>

**** DESCRIBE MESH(ES) ****
Coarse mesh:
   1. Number of meshpoints :  32
   2. Fraction of 2*PI/A0  : 1.000

Fine mesh:
   3. Fine mesh is generated.
   4. Number of meshpoints :   2
   5. Fraction of 2*PI/A0  : 1.000

ENTER SELECTION (0=EXIT) :
<2><ENTER>

Enter fraction :
<0.24><ENTER>

**** DESCRIBE MESH(ES) ****
Coarse mesh:
```

```
   1. Number of meshpoints :  32
   2. Fraction of 2*PI/A0  :  .240

Fine mesh:
   3. Fine mesh is generated.
   4. Number of meshpoints :   2
   5. Fraction of 2*PI/A0  : 1.000

ENTER SELECTION (0=EXIT) :
<4><ENTER>

Enter number of fine meshpoints : 24

**** DESCRIBE MESH(ES) ****
Coarse mesh:
   1. Number of meshpoints :  32
   2. Fraction of 2*PI/A0  :  .240

Fine mesh:
   3. Fine mesh is generated.
   4. Number of meshpoints :  24
   5. Fraction of 2*PI/A0  : 1.000

ENTER SELECTION (0=EXIT) :
<5><ENTER>

Enter fraction : 0.06

**** DESCRIBE MESH(ES) ****
Coarse mesh:
   1. Number of meshpoints :  32
   2. Fraction of 2*PI/A0  :  .240

Fine mesh:
   3. Fine mesh is generated.
   4. Number of meshpoints :  24
   5. Fraction of 2*PI/A0  :  .060

ENTER SELECTION (0=EXIT) :
<0><ENTER>
```

Selection 3: SET WHICH BANDS TO CALCULATE

Here you specify for which bands the data should be stored. The program calculates energies and eigenvectors for all bands, but usually different meshes are wanted for different bands, so you may run the program once for each band without storing results for the bands in which you have no interest at the time. The current setting is shown on the screen, and

you must specify for each band wether it should be stored or not:

```
**** SET WHICH BANDS TO CALCULATE ****

Currently results are stored for bands :  1   3
Should results for band 1 be stored ? (Y/N)
<N><ENTER>
Should results for band 2 be stored ? (Y/N)
<N><ENTER>
Should results for band 3 be stored ? (Y/N)
<Y><ENTER>
```

Selection 4: SET WHAT TO CALCULATE

The user may also select which quantities to compute. How to do it, is obvious from the example:

```
**** SET WHAT TO CALCULATE ****

Current setting :          EIGENVECTORS    GRADIENTS     ENERGIES

Should energies be calculated ? (Y/N) :
<Y><ENTER>
Should gradients be calculated ? (Y/N) :
<Y><ENTER>
Should second derivatives be calculated ? (Y/N) :
<Y><ENTER>
Should eigenvectors be calculated ? (Y/N) :
<N><ENTER>
```

Selection 5: DEFINE FILENAMES

The user may change the names of the output files. A survey of the current setting is written on the screen. You select for which band you want to change the filename by typing the corresponding number. Then you respond to the prompts for the new filnames. The filename remains unchanged if you respond with <ENTER> only. The program then outputs the new setting, and you may change more filenames or return to the main menu by entering a "0".

```
**** DEFINE FILENAMES ****
Filenames
              Energies        Gradients       Sec. deriv.     Eigenvectors
1. Band 1:
2. Band 2:    LHEN.TAB        LHGR.TAB        LHSD.TAB        LHVE.TAB
3. Band 3:    HHENU.TAB       HHGRU.TAB       HHSDU.TAB       HHVEU.TAB

WHICH DO YOU WANT TO CHANGE (0=NONE) ?
```

```
<2><ENTER>
New filenames for band2
Enter name of energy file [LHEN.TAB] :
LHENU.TAB
Enter name of gradient file [LHGR.TAB] :
LHGRU.TAB
Enter name of sec. derivative file [LHSD.TAB] :
LHSDU.TAB
Enter name of eigenvector file [LHVE.TAB] :
LHVEU.TAB

**** DEFINE FILENAMES ****
Filenames
              Energies       Gradients      Sec. deriv.    Eigenvectors
1. Band 1:
2. Band 2:    LHENU.TAB      LHGRU.TAB      LHSDU.TAB      LHVEU.TAB
3. Band 3:    HHENU.TAB      HHGRU.TAB      HHSDU.TAB      HHVEU.TAB

WHICH DO YOU WANT TO CHANGE (0=NONE) ?
```

Selection 6: SHOW ALL DATA

This selection provides a survey of the current setting of all parameters. The example below shows what the output will look like when the input has been done as in the previous examples.

```
**** SHOW ALL DATA ****

Strain:         .0000000   .0000000   .0000000
                .0000000   .0000000   .0000000
                .0000000   .0000000   .0000000

Coarse mesh:
   Number of meshpoints :  32
   Fraction of 2*PI/A0  :  .240

Fine mesh:
   Fine mesh is generated.
   Number of meshpoints :  24
   Fraction of 2*PI/A0  :  .060


Results are stored for bands :                3

The program calculates :                   GRADIENTS     ENERGIES  SEC. DERIV.
```

```
Filenames:
              Energies       Gradients      Sec. deriv.    Eigenvectors
   Band 1:
   Band 2:    LHENU.TAB      LHGRU.TAB      LHSDU.TAB      LHVEU.TAB
   Band 3:    HHENU.TAB      HHGRU.TAB      HHSDU.TAB      HHVEU.TAB

PRESS ENTER TO RETURN...
```

Selection 7: SAVE AND QUIT

This is the exit to the operating system. No data is saved until this selection is entered. The output below is shown on the screen.

```
**** SAVE AND QUIT ****

Data written to file "KPBAND.INI".
```

E.1.2 How to run KPBAND.

It is rather straightforward to run KPBAND. The only requirements for the program to run is that the initialization file is present on the disk, and that there is enough disk space to hold the output files. KPBAND does not require any keyboard input. This makes it easy to run it as a batch job on machines with such capabilities. For information purposes some output is given to the screen. This output should be redirected to a file when the program is run as a batch job. On some computers , VAX for instance, this is done automatically. The output files are those specified in the initialization file. Be aware that the required disk space grows quickly with increasing number of meshpoints along an axis. An example of a typical screen output is shown below.

```
**************** KPBAND ****************
Program calculating bandstructure and
related quantities for GaAs.

Strain:       0.0000000  0.0000000  0.0000000
              0.0000000  0.0000000  0.0000000
              0.0000000  0.0000000  0.0000000

Coarse mesh:
   Number of meshpoints :  32
   Fraction of 2*PI/A0  : 0.240

Fine mesh:
   Fine mesh is generated.
   Number of meshpoints :  24
   Fraction of 2*PI/A0  : 0.060
```

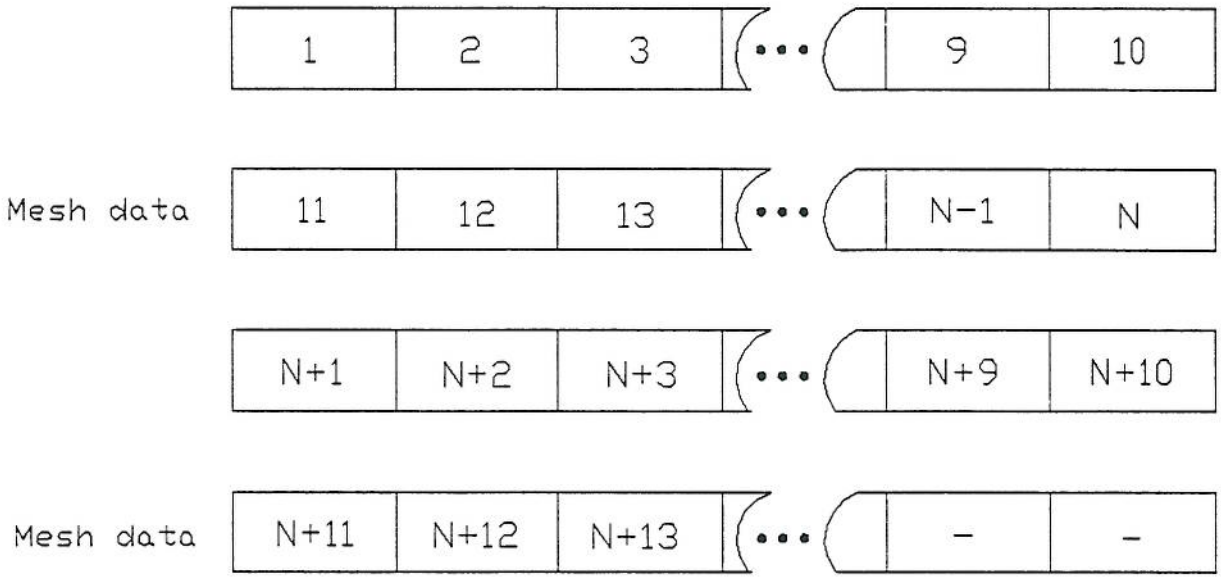

Figure E.1: KPBAND file format.

The contents of the other records may differ for different filetypes. For energy files record nr. 6 contains the highest energy entirely enclosed by the mesh.

All floating point data is written to file in single precision. This means that each record is 4 bytes for energy files, 12 bytes for gradient files, 24 bytes for second derivatives files and 96 bytes for eigenvector files. The eigenvectors are stored as two complex six component vectors in sequence. First and second derivatives are stored in the order x,y,z and xx,yy,zz,xy,xz,yz respectively.

E.2 SCRATES user guide.

SCRATES is a program for calculating scattering rates for holes in GaAs numerically. It is based on an extrapolation algorithm using a uniform mesh of energies and energy gradients as input data. The input files are equivalent to the corresponding output files of KPBAND. The rates are output in an equivalent file format.

The scattering mechanisms implemented are:

- Polar optical scattering, absorption and emission
- Nonpolar optical scattering, absorption and emission
- Acoustic deformation potential scattering, absorption and emission
- Ionized impurity scattering

The overlap factors are calculated separately and in three different ways:

- Unity overlap factor. Applicable to conduction band electrons in the lower energy regime or where the overlap factor does not enter as a multiplicative factor.
- Analytical expressions given by Wiley. These are applicable to light and heavy holes in unstrained cubic semiconductors.
- Overlap factors calculated from eigenvectors of the 6×6 $\vec{k}\cdot\vec{p}$ hamiltonian and applicable to holes in both strained and unstrained semiconductor.

The scattering rates are stored as a uniform mesh in k-space. If the file with initial states contains a fine mesh, this will also be generated for the rates. The setup of a program run is done from a separate program call SCRINI in order to make it easy to run SCRATES as a batch job. Through SCRINI the user may control what is calculated by SCRATES and to a certain extent how this is done. The following sections describes how to set up and run SCRATES.

E.2.1 How to set up SCRATES.

The set up of the program by SCRINI is controlled by a simple menu system. The program tries to read an initialization file from the disk just after start up. If this fails, two messages appear on the screen before the main menu is displayed. They are:

```
NO INITIALIZATION FILE IS FOUND

FILE "SCRATES.INI" HAS BEEN CREATED
```

A initialization file has then been created with a few parameters set to default values, and others undefined. If an initialization file is found the program reads it, and the user may change the setting. The main menu has the following appearance on the screen:

```
....SCRINI MAIN MENU.....

YOU MAY :
 1. CHANGE SCATTERING MECHANISM
 2. CHANGE TEMPERATURE
 3. CHANGE INITIAL AND FINAL BANDS
 4. CHANGE FILENAMES
 5. ALTER NAMES AND NUMBER OF BANDS
 6. SHOW ALL DATA
 7. SPECIFY HOW TO CALCULATE OVERLAP IN
 8. SAVE AND EXIT

ENTER SELECTION:
```

A selection is done by typing its number and pressing <ENTER>. Below each selection is described one by one. The menues are rather self explanatory so only brief comments to the examples are given.

Selection 1: CHANGE SCATTERING MECHANISM

The alternatives appear on the screen and the program returns to the main menu just after a selection is done.

```
....CHANGE SCATTERING MECHANISM....

THE CURRENT SCATTERING MECHANISM IS : IONIZED IMPURITY SCATTERING

THE AVAILABLE SCATTERING MECHANISMS ARE:
 1. POLAR OPTICAL, ABSORPTION
 2. POLAR OPTICAL, EMISSION
 3. NONPOLAR OPTICAL, ABSORPTION
 4. NONPOLAR OPTICAL, EMISSION
 5. ACOUSTIC DEFORMATION POTENTIAL, ABSORPTION
 6. ACOUSTIC DEFORMATION POTENTIAL, EMISSION
 7. IONIZED IMPURITY SCATTERING

ENTER SELECTION (0=UNCHANGED):
<7> <ENTER>
```

Selection 2: CHANGE TEMPERATURE

Here you set the crystal temperature. The old value is displayed, and you must enter a new one-

```
....CHANGE TEMPERATURE....

THE CURRENT TEMPERATURE IS  77.00 K

ENTER NEW TEMPERATURE [K] :
<300> <ENTER>
```

Selection 3: CHANGE INITIAL AND FINAL BANDS

Here you specify in which band the initial and final states are to be found. Because there are several files connected with each band, each band is given a name which is referred to here. The names are defined by choosing selection 5 and the filenames are defined under selection 4. The specification of initial and final bands can not be done if the bands are not previously defined.

```
....CHANGE INITIAL AND FINAL BANDS....

THE CURRENT SETTING IS :
1. INITIAL BAND :  NOT DEFINED
2. FINAL BAND   :  NOT DEFINED

WHICH DO YOU WANT TO CHANGE (0=NONE) ?
<1> <ENTER>
THE POSSIBLE INITIAL BANDS ARE :
```

```
 1. LIGHT HOLE BAND
 2. HEAVY HOLE BAND

MAKE A SELECTION (0=NONE) :
<2> <ENTER>

....CHANGE INITIAL AND FINAL BANDS....

THE CURRENT SETTING IS :
1. INITIAL BAND :  THE HEAVY HOLE BAND
2. FINAL BAND   :  NOT DEFINED

WHICH DO YOU WANT TO CHANGE (0=NONE) ?
<2> <ENTER>
THE POSSIBLE FINAL BANDS ARE :
 1. LIGHT HOLE BAND
 2. HEAVY HOLE BAND

MAKE A SELECTION (0=NONE) :
<1> <ENTER>

....CHANGE INITIAL AND FINAL BANDS....

THE CURRENT SETTING IS :
1. INITIAL BAND :  THE HEAVY HOLE BAND
2. FINAL BAND   :  THE LIGHT HOLE BAND

WHICH DO YOU WANT TO CHANGE (0=NONE) ?
<0> <ENTER>
```

Selection 4: CHANGE FILENAMES

Here you define the filenames for each band and the name of the ouptut file. If you don't calculate overlapfactors from eigenvectors you may enter a dummy name for eigenvector files. Also gradients are not needed for the initial band and can be assigned a dummy name if its desirable.

```
....CHANGE FILENAMES....

THE FILENAMES ARE:
                                  ENERGIES      GRADIENTS      EIGENVECTORS

 1.           LIGHT HOLE BAND :
 2.           HEAVY HOLE BAND :  HHEN.TAB      HHGR.TAB       HHVE.TAB

 3. OUTPUT FILE : SCRAT.TAB
```

```
WHICH DO YOU WANT TO CHANGE (0=NONE) ?
<1> <ENTER>
NEW FILENAMES FOR THE LIGHT HOLE BAND.
ENTER ENERGY FILE NAME :
<LHEN.TAB> <ENTER>
ENTER GRADIENT FILE NAME :
<LHGR.TAB> <ENTER>
ENTER EIGENVECTOR FILE NAME :
<LHVE.TAB> <ENTER>

....CHANGE FILENAMES....

THE FILENAMES ARE:
                                  ENERGIES      GRADIENTS     EIGENVECTORS

 1.           LIGHT HOLE BAND :  LHEN.TAB      LHGR.TAB      LHVE.TAB
 2.           HEAVY HOLE BAND :  HHEN.TAB      HHGR.TAB      HHVE.TAB

 3. OUTPUT FILE : SCRAT.TAB

WHICH DO YOU WANT TO CHANGE (0=NONE) ?
<0> <ENTER>
```

Selection 5: ALTER NAMES AND NUMBER OF BANDS

There are four possible choices here:

```
....ALTER NAMES AND NUMBER OF BANDS....

YOU MAY :
 1. RENAME BAND
 2. ADD BAND
 3. DISCARD BAND
 4. LIST BANDS

ENTER SELECTION (0=NONE):
```

You define a new band by selecting no. 2: "ADD BAND". Then the name of the new band is prompted for. It is possible to have five bands defined at the same time. If you want to give a band another name you choose no. 1: "RENAME BAND". The currently defined bands are then listed and you may choose to rename one of them. Alternative 3 is chosen if you want to remove a band. All the defined bands are listed and you choose one (or none) to be discarded. Then all its filenames are discarded. If it is previously set to be the initial or final band this will now be undefined. Typing 4, "LIST BANDS", just displays a list of the defined bands on the screen. A typical input sequence can be as shown below:

```
....ALTER NAMES AND NUMBER OF BANDS....
```

```
YOU MAY :
 1. RENAME BAND
 2. ADD BAND
 3. DISCARD BAND
 4. LIST BANDS

ENTER SELECTION (0=NONE):
<2> <ENTER>
ENTER NAME OF NEW BAND:
HEAVY HOLE

....ALTER NAMES AND NUMBER OF BANDS....

YOU MAY :
 1. RENAME BAND
 2. ADD BAND
 3. DISCARD BAND
 4. LIST BANDS

ENTER SELECTION (0=NONE):
<4> <ENTER>

THE BANDS DEFINED ARE:
 1. LH
 2. HEAVY HOLE

....ALTER NAMES AND NUMBER OF BANDS....

YOU MAY :
 1. RENAME BAND
 2. ADD BAND
 3. DISCARD BAND
 4. LIST BANDS

ENTER SELECTION (0=NONE):
<1> <ENTER>

YOU MAY RENAME :
 1. LH
 2. HEAVY HOLE
ENTER SELECTION (0=NONE):
<1> <ENTER>
ENTER NEW NAME :
LIGHT HOLE
```

Selection 7: SPECIFY HOW TO CALCULATE OVERLAP IN

Here you decide how to calculate overlap integrals. If you choose alternative 2, SCRATES will use the intraband expression if the initial and final bands are the same, otherwise the interband expression is used. This means that you can't use the analytical overlap factors on two different meshes for the same band.

```
....SPECIFY HOW TO CALCULATE THE OVERLAP INTEGRAL....


THERE ARE THREE ALTERNATIVES :
 1. BY EIGENVECTORS OF 6x6 Kohn-Luttinger HAMILTONIAN
 2. BY ANALYTICAL EXPRESSIONS AFTER Wiley
 3. BY ASSUMING UNITY OVERLAP INTEGRAL

ENTER SELECTION :
<1> <ENTER>
```

Selection 6: SHOW ALL DATA

This selection provides a survey of all the parameter settings. If data is entered as described above the screen output will have the following appearance:

```
....SHOW ALL DATA....

THE CURRENT SCATTERING MECHANISM IS : POLAR OPTICAL, ABSORPTION
THE CURRENT TEMPERATURE IS 300.00 K
INITIAL BAND :  THE HEAVY HOLE BAND
FINAL BAND   :  THE LIGHT HOLE BAND
THE FILENAMES ARE:
                                ENERGIES      GRADIENTS     EIGENVECTORS
              LIGHT HOLE BAND :  LHEN.TAB      LHGR.TAB      LHVE.TAB
              HEAVY HOLE BAND :  HHEN.TAB      HHGR.TAB      HHVE.TAB
THE OVERLAP INTEGRAL IS CALCULATED BY EIGENVECTORS OF 6x6 Kohn-Luttinger HAMILT
ONIAN
OUTPUT FILE : SCRAT.TAB

PRESS RETURN TO CONTINUE
```

Selection 8: SAVE AND EXIT

Making this selection causes the program to save all data and exit. If everything works well the output looks like this:

```
...SAVE AND EXIT...

DATA SAVED ON FILE "SCRATES.INI"
```

Before program termination there is a check on wether the information is sufficient for a run of SCRATES. If it is not found to be sufficient, some warnings are given. The possible warnings are:

```
SCRINI WARNING : SCATTERING MECHANISM ISN'T SET
SCRINI WARNING : INITIAL BAND IS NOT DEFINED
SCRINI WARNING : FINAL BAND IS NOT DEFINED
SCRINI WARNING : ENERGY FILE FOR INITIAL BAND IS NOT DEFINED
SCRINI WARNING : GRADIENT FILE FOR INITIAL BAND IS NOT DEFINED
SCRINI WARNING : EIGENVECTOR FILE FOR INITIAL BAND IS NOT DEFINED
SCRINI WARNING : ENERGY FILE FOR FINAL BAND IS NOT DEFINED
SCRINI WARNING : GRADIENT FILE FOR FINAL BAND IS NOT DEFINED
SCRINI WARNING : EIGENVECTOR FILE FOR FINAL BAND IS NOT DEFINED
SCRINI WARNING : NO OUTPUT FILE IS DEFINED
```

E.2.2 How to run SCRATES.

To run SCRATES you must ensure that SCRATES.INI is present on the disk together with the input files needed. The program gives output about what is done during the run. No keyboard input is necessary so the program can be run as a batch job. If the set up has been done as described above, the output will be:

```
****************** SCRATES ******************
Program for numerical calculation of scattering
rates with discretized band structure.

SCATTERING MECHANISM IS : POLAR OPTICAL, ABSORPTION
TRANSITION FROM : HEAVY HOLE
             TO : LIGHT HOLE
AT TEMPERATURE :      300.000000 K
OVERLAP INTEGRAL IS CALCULATED FROM EIGENVECTORS
INPUT FILES FOR INITIAL STATES ARE:
HHEN.TAB
HHGR.TAB
HHVE.TAB
INPUT FILES FOR FINAL STATES ARE:
LHEN.TAB
LHGR.TAB
LHVE.TAB
OUTPUT FILE IS : SCRAT.TAB
READING DATA FOR FINAL STATES.
COARSE MESH :
ENERGIES...
GRADIENTS...
EIGENVECTORS...
FINE MESH :
ENERGIES...
GRADIENTS...
EIGENVECTORS...
COMPLETED.
```

```
CREATING MIN/MAX TABLES FOR FINAL STATES...
COARSE MESH...
FINE MESH...
COMPLETED.
COMPUTING RATES:
COARSE MESH...
100% COMPLETED
FINE MESH...
100% COMPLETED
```

When the initialization file is not found, or when it can't be read for some reason, the program will give a message about it and terminate:

```
****************** SCRATES ******************
Program for numerical calculation of scattering
rates with discretized band structure.

SCRATES ERROR : ERROR READING INITIALIZATION FILE "SCRATES.INI"
Stop - Program terminated.
```

If the data in SCRINI is improperly specified the program will give error messages and terminate. The possible error messages are:

```
SCRATES ERROR : SCATTERING MECHANISM IS UNDEFINED.
SCRATES ERROR : INITIAL BAND IS UNDEFINED
SCRATES ERROR : FINAL BAND IS UNDEFINED
SCRATES ERROR : ENERGY FILE FOR INITIAL BAND IS UNDEFINED
SCRATES ERROR : GRADIENT FILE FOR INITIAL BAND IS UNDEFINED
SCRATES ERROR : EIGENVECTOR FILE FOR INITIAL BAND IS UNDEFINED
SCRATES ERROR : ENERGY FILE FOR FINAL BAND IS UNDEFINED
SCRATES ERROR : GRADIENT FILE FOR FINAL BAND IS UNDEFINED
SCRATES ERROR : EIGENVECTOR FILE FOR FINAL BAND IS UNDEFINED
SCRATES ERROR : OUTPUT FILE IS UNDEFINED
```

Also there is a check on wether the input files are consistent or not. If the gradient or eigenvector files are found to have another mesh than the energy file for a band an error message is given. It will be on the form:

```
SCRATES ERROR : INCONSISTENT INPUT FILE "filename"
```

If the input files for final states are to big to fit the internal arrays, an error message will be given on the form:

```
SCRATES ERROR : TO BIG INPUT FILE "filename"
```

Any detected error will cause the program to terminate. The error checking is not foolproof, but detects and reports the most common errors so the user will know what's going wrong in most cases.

E.2.3 File format

The file structure is exactly the same as for KPBAND. The rates are stored in 4 byte records and the housekeeping data is the same as for KPBAND , except that no rate is calculated for $\vec{k} = 0$ and that the value of $\frac{2\pi}{a_0}$ is not stored.

References

[1] H. Shichijo and K. Hess, Phys. Rev. **B23**, 4197 (1981)

[2] K. Brennan and K. Hess, Phys. Rev. **B29**, 5581 (1984)

[3] M. V. Fischetti and S. Laux, Phys. Rev. B **38**, 9721 (1988)

[4] J. M. Hinckley and J. Singh, Appl. Phys. Lett. **53**, 785 (1988)

[5] P. J. Price, Semiconductors and Semimetals **14**, 249 (1979)

[6] C. Jacoboni and L. Reggiani, Rew. Mod. Phys **55**, 645 (1983)

[7] G. L. Bir and G. E. Pikus, Symmetry and Strain-induced Effects in Semiconductors, Keter Publishing House Jerusalem Ltd. , 1974

[8] E. O. Kane, Semiconductors and Semimetals **1**, Academic Press, New York, 1966

[9] J. M. Luttinger and W. Kohn, Phys. Rev. **97**, 869 (1955)

[10] J. D. Wiley, Semiconductors and Semimetals **10**, Academic Press, New York, 1975
or
J. D. Wiley, Phys. Rev. **B4**, 2485 (1971)

[11] E. O. Kane, J. Phys. Chem. Solids **1**, 249 (1957)

[12] G. Gilat and L. J. Raubenheimer, Phys. Rev. **144**, 390 (1966)

[13] T. Brudevoll, T. A. Fjeldly, J. Baek and M. Schur, J. Appl. Phys. **67**, 7373 (1990)

[14] M. O. Vassell, A. K. Ganguly and E. M. Conwell, Phys. Rev. **B2**, 948 (1970)

[15] P. Lawætz, The influence of holes on the phonon spectrum of semiconductors, The Technical University of Denmark, Lyngby, Denmark

[16] P. Lawætz, Phys. Rev. B4, 3460 (1971)

[17] Manuel Cardona, J. Phys. Chem. Solids **24**, 1543 (1963)

[18] NAG workstation library handbook, Numerical Algorithms Group Limited, Oxford, United Kingdom, 1986

[19] M. Cardona and F. H. Pollak, Phys. Rev. **142**, 530 (1965)

[20] P. Lawætz, Some transport properties of holes in germanium, The Technical University of Denmark, Lyngby, Denmark, 1967.

[21] G. L. Bir and G. E. Pikus, Soviet Physics Solid State **2**, 2039 (1961)